Sexual-dimorphism in human immune system aging

Eladio J. Márquez[1], Cheng-han Chung[1], Radu Marches[1], Robert J. Rossi[1], Djamel Nehar-Belaid[1], David J Mellert[1], George A Kuchel[2*], Jacques Banchereau[1*], Duygu Ucar[1*]

[1]The Jackson Laboratory for Genomic Medicine, Farmington, CT, 06030, USA.

[2]University of Connecticut Center on Aging, UConn Health Center, Farmington, CT, 06030, USA.

[*]These senior authors contributed equally to this work.

Correspondence: duygu.ucar@jax.org

Abstract

Sex differences in immune functions and responses contribute to health- and life-span disparities between men and women. However, the role of sex on immune system aging is not well understood. To fill this gap, we studied peripheral blood mononuclear cells (PBMCs) from 194 healthy adults (100 women, 94 men) ranging from 22-93 years old using ATAC-seq, RNA-seq, and flow cytometry technologies. These data revealed a shared epigenomic signature of aging between sexes composed of declines in naïve T cell functions and increases in monocyte and cytotoxic cell functions. These changes were greater in magnitude in men. Additionally, we uncovered male-specific decreases in expression/accessibility of B-cell associated loci. Age-related epigenomic changes were more abrupt at two timepoints in the human lifespan. The first timepoint was similar between sexes in terms of timing (early forties) and magnitude. In contrast, the latter timepoint was earlier (~5 years) and more pronounced in men (mid-sixties versus late-sixties). Unexpectedly, differences between men and women PBMCs increased after 65 years of age, with men having higher monocyte and pro-inflammatory activity and lower B/T cell activity compared to women. Our study uncovered which immune cell functions and molecules are differentially affected with age between sexes, including the differences in timing and magnitude of changes, therefore providing an invaluable resource for tailoring therapies to extend health- and life-span in the clinic (https://shinyapps.jax.org/44c0a53ebb13f7fd5e2ddbced1a37f51/).

Keywords: immunosenescence, sexual dimorphism, inflammation, aging, immune system

Introduction

Human blood peripheral blood mononuclear cells (PBMCs) undergo both cell-intrinsic and cell-compositional changes (i.e., cell frequencies) with age, where certain immune functions are impaired and others are remodeled[1]. Analyses of human blood samples have uncovered significant aging-related changes in gene expression[2] and DNA methylation levels[3]. More recent studies revealed that chromatin accessibility of purified immune cells, especially $CD8^+$ T cells, also change significantly with aging, impacting the activity of important receptor molecules, signaling pathways, and transcription factors (TF)[4,5]. Together, these changes likely contribute to aging-related immunodeficiency and ultimately to increased frequency of morbidity and mortality among older adults. However, it is not clear to what extent these aging-associated changes are shared between men and women.

It is well established that immune systems of men and women function and respond to infections and vaccination differently[6]. For example, 80% of autoimmune diseases occur in women, who typically show stronger immune responses than males[7]. Stronger responses in women produce faster clearance of pathogens and better vaccine responsiveness, but also contribute to women's increased susceptibility to inflammatory and autoimmune diseases. Although not systematically described, these differences likely stem from differences in both cell frequencies and cell-intrinsic programs. For example, a study conducted in a small cohort of young individuals showed that women have more B cells (both percentage and absolute cell counts) in their blood compared to men[8]. In addition, hundreds of genes are differentially expressed between young men and young women in sorted B cells[9]. A recent study more comprehensively described sex-biased transcripts in purified immune cells (n=1,800), the majority of which were autosomal genes[10]. Furthermore, consortium projects have uncovered age- and sex-dependent differences in immune responses to stimuli[11,12]. Despite the importance of both sex and age in shaping immune cell functions and responses, it is not known whether men's and women's immune systems go through similar changes over human lifespan, and whether these changes occur at the same time and at the same rate.

To comprehensively study this, we profiled PBMCs of healthy adults by carefully matching the ages of male and female donors. By developing novel computational pipelines for functional enrichments, trajectory and breakpoint analyses, we uncovered and compared immune system aging signatures in men and women, including longitudinal trends in the genomics data. These findings significantly advanced our understanding of in which ways aging differentially affects the immune systems of men and women.

Profiling PBMCs of healthy adults

We recruited 194 community-dwelling healthy research volunteers (100 women, 94 men) spanning the adult lifespan (22 to 93 years old) (**Fig. 1a**, **Table S1**). Our cohort was composed of 56 young (ages 22-40: 23 men, 33 women), 68 middle-aged (ages 41-64: 36 men, 32 women), and 70 older subjects (65+: 35 men, 35 women). No significant differences were detected between sexes in their frailty scores or in the age distributions across decades (**Fig. S1g, Table S1**). PBMCs were profiled using ATAC-seq (n=120: 54 men, 66 women), RNA-seq (n=75: 41 men, 34 women), and flow cytometry (n=129: 61 men, 68 women) techniques (**Table S1**).

Aging is the main driver of variation in PBMC ATAC-seq and RNA-seq data

To identify the major sources of variation in the genomics data, we, first, conducted principal component analyses (PCA) using open chromatin regions (OCRs; n=78,167) and expressed genes (n=12,350) using

all samples that pass quality control (100 ATAC-seq and 74 RNA-seq samples) (**Table S2**). The first principal component (PC1) captured 15% of the variation in ATAC-seq data and 18.6% of the variation in RNA-seq data and in both datasets was associated with age groups, where PC1 scores of young and older individuals significantly differed (**Figs. 1b, S1a, S1b**, **Table S3**). Interestingly, differences in PC1 scores of age groups were more significant in men in both ATAC-seq ($p<0.05$ for women, $p<0.001$ for men) and RNA-seq data (p=N.S. for women, p=0.03 for men), suggesting that aging has a larger impact on male PBMCs (**Fig. 1b**). The functional annotation of PC1-related genes based on immune modules[13] revealed losses in chromatin accessibility/gene expression levels associated with the 'T cell' module and uncovered gains in chromatin accessibility/gene expression levels associated with 'myeloid lineage' and 'inflammation' (**Fig. 1c**), confirmed by single-cell driven gene set enrichment analyses (**Fig. S1c**). Together, these analyses suggest that aging is the main driver of variation in PBMC epigenomes/transcriptomes, where age-related variation is negatively associated with naïve T cells and positively associated with myeloid lineage and inflammation, in agreement with the two signatures of immune system aging: immunosenescence and inflamm-aging[14].

Aging-related changes in PBMC cell compositions

Using flow cytometry, we quantified the frequencies of four major cell populations within PBMCs: $CD4^+$ and $CD8^+$ T cells, $CD19^+$ B cells, and $CD14^+$ monocytes from 130 individuals (68 women, 62 men) (**Table S4**). Among these, the proportions of $CD8^+$ T cells were the most significantly affected with age in agreement with our previous study[5], where a significant decline was observed both in male ($p=8.2e^{-07}$) and female PBMCs (p=0.0065) with age (**Fig. 1d**). Similarly, the percentage of $CD4^+$ T cells declined with age both in males (p=0.01) and females (p=0.0047). In contrast, we detected a male-specific decline in B cell proportions after age 65 ($p=1.6e^{-05}$ for men, p=0.11 for women), which led to a significant difference in B cell proportions between older men and older women (p=0.0032, median: 4.15% for women, 3.15% for men) (**Fig. 1d, Table S4**). In contrast, we did not detect significant aging- or sex-related changes in the proportions of $CD14^+$ monocytes (Kruskal-Wallis p-value to compare all groups = 0.44) (**Fig. 1d**).

We also quantified the frequencies of $CD4^+$ and $CD8^+$ T cell subsets in a subgroup of young and older individuals (n=81): naïve ($CD45RA^+$, $CCR7^+$), central memory ($CD45RA^-$, $CCR7^+$), effector memory ($CD45RA^-$, $CCR7^-$), and effector memory RA ($CD45RA^+$, $CCR7^-$). As expected, frequencies of naïve T cells decreased with age, where declines were more significant in the $CD8^+$ T cell compartment in both sexes (**Figs. S1d, S1e**). As previously reported[15], we observed that women on average had more naïve T cells compared to men. For example, on average 13.1% of PBMCs were naïve $CD4^+$ T cells in young women, compared to 7.8% in young men (p=0.00052) (**Table S4**). A recent study showed that women

have elevated thymic function compared to men at all ages[16], potentially explaining the differences in naïve T cell frequencies. Sex- and age-related changes in other T cell subsets (central, effector memory, and effector cells) were also observed. However, these were not as significant and as consistent as the changes observed in the naïve T cell compartment (**Figs. S1d, S1e**).

Using generalized linear models (GLM), we quantified the relationship between the age and sex of individuals and the variation in their PBMC compositions, thus confirming that age is most strongly associated with the changes in $CD8^+$ T cell proportions, especially naïve $CD8^+$ T cells (**Fig. S1f**). Whereas, sex is most strongly associated with the variation in naïve $CD4^+$ T cells; women have higher proportions compared to men (**Figs. S1d, S1f**). Finally, we observed that B cell proportions are significantly associated with joint effects of sex and age (i.e., the interaction term in models) (**Fig. S1f**), due to the male-specific decline in B cell proportions after age 65 (**Fig. 1d**). Together, these data and analyses uncovered shared and sex-specific changes in cell compositions with age, some of which may underlie aging-related genomic changes in PBMCs.

Shared and sex-specific chromatin accessibility signatures of aging

Using GLM models, we detected ATAC-seq peaks that are differentially accessible (DA) between young and older individuals[17] at FDR 5%. In men, 10,196 peaks were DA with age (13% of all tested peaks: 5,782 closing, 4,414 opening), compared to 4,516 DA peaks in women (5.8% of tested: 3,309 closing, 1,207 opening) (**Fig. 2a, Table S5**). DA peaks in men and women significantly overlapped, despite the presence of thousands of sex-specific loci associated with aging (**Fig. S2a**, $p<2e-308$ for closing, $p=2.2e-19$ for opening peaks). Furthermore, a positive and significant correlation was detected between men and women in terms of age-related epigenomic changes in their PBMCs ($r=0.445$, $p<0.001$). DA peaks corresponded to 6612 and 3634 genes in men and women, respectively, based on their distance to transcription start sites (TSS; **Fig. S2a**). Functional annotation of these peaks using Roadmap chromatin states in immune cell subsets[18] (i.e., $CD14^+$ monocytes, $CD19^+$ B cells, $CD56^+$ NK cells, naïve and memory $CD4^+$ and $CD8^+$ T cells) revealed that closing peaks were mostly composed of regulatory elements (i.e., promoters and enhancers) shared across immune cells, especially in T cell subsets (**Figs. 2b, S2b**). On the other hand, opening peaks were mostly composed of enhancers active in $CD14^+$ monocytes and $CD56^+$ NK cells in both sexes (**Fig. 2b, S2c**). Consistent with our previous findings[5], there were more 'quiescent' loci (i.e., loci with no known functional annotation) among opening peaks than closing peaks, which may be partially due to global chromatin deregulation with aging[19].

To identify immune cells/functions most affected by aging, we studied epigenomic changes at cell-specific loci (i.e., loci annotated as promoters/enhancers only in one cell type) (**Fig. S2b**). In both sexes, opening peaks were more likely to be associated with monocyte-, NK, and memory $CD8^+$ cell-specific loci, whereas closing peaks were mostly associated with naïve $CD4^+$ and naïve $CD8^+$ T cell-specific loci (**Figs. 2c, S2d, S2e**). Despite these similarities between sexes, we observed that a greater number of cell-specific loci were affected with aging in men. Most notably, there were 960 monocyte-specific peaks that significantly gained accessibility with aging in men, whereas only 64 such loci were detected in women. Only B cells showed the opposite epigenomic remodeling pattern with aging between sexes, where B cell-specific regulatory elements were more likely to be among opening peaks in women and among closing peaks in men (**Fig. 2c**). Overall fold change distributions and enrichment analyses based on cell-specific loci confirmed these results, with opening peaks being enriched in monocyte and cytotoxic cell loci, and closing peaks enriched in naïve T cell loci (**Figs. S2d, S2e**). In contrast, closing peaks were enriched in B cell-specific regulatory elements only in men, suggesting a male-specific decline in the B cell compartment with aging (**Figs. S2d, S2e**). Furthermore, immune module[13,20] and WikiPathways enrichment analyses uncovered that inflammation related modules/pathways were associated to chromatin opening in both sexes (**Table S6**) (e.g., Inflammation I module, MyD88 cascade initiated on plasma membrane (WP2801) pathway). On the other hand, in both sexes, closing peaks were significantly associated to modules/pathways related to T cell signaling and functions, notably including the IL-7 Signaling pathway (WP205) in agreement with our previous study[5]. Several molecules in this pathway were associated to chromatin closing in both sexes including *IL7R*, *JAK1*, *STAT5B* and *PTK2B* (**Table S6, Fig. 2d**). Together, these results suggest that there is an epigenomic signature of aging shared between sexes, which include gains in chromatin accessibility for pro-inflammatory processes, monocytes and cytotoxic cells (NK and $CD8^+$ memory T cells) and losses in accessibility for naïve T cells. Interestingly, these changes were even more pronounced in men, despite the fact that male and female cohorts were comparable in terms of distributions of chronological ages, frailty scores, and numbers of individuals in each group (**Fig. S1g, Table S1**). Furthermore, we discovered that B cells age differently between sexes, where a significant loss in chromatin accessibility was detected only in men.

Correlated aging-related changes in transcriptomes and epigenomes

By comparing PBMC RNA-seq data from young and older individuals, we identified 918 differentially expressed (DE) genes in women (539 up and 379 down) and 791 genes in men (510 up and 281 down) at FDR 10%[17] (**Fig. S3a, Table S7**). These DE genes overlapped significantly between sexes. For example, 201 downregulated genes were shared between sexes (p-value=8.12e-149) and included important molecules for T cell functions (e.g., *TCF7*, *LEF1*, *CCR7*) (**Fig. S3b, Table S7**). The annotation of these

genes using cell-specific marker genes from single cell RNA-seq (scRNA-seq) data in PBMCs and sorted cell RNA-seq data[10], revealed that the genes upregulated with aging were most significantly enriched in marker genes for NK cells in both sexes (**Fig. 2e**), also included marker genes for monocytes and activated $CD8^+$ T cells (**Figs. S3c, S3d, Table S8**). In contrast, downregulated genes were most significantly enriched in naïve T cell marker genes (e.g., *CD27*, *CCR7*, *LEF1*) in both sexes (**Figs. 2e, 2f, Table S8**). Similar to the ATAC-seq data (**Fig. 2c**), aging-related gene expression changes in the B cell compartment were sex dimorphic. B cell-specific genes, especially naïve B cell genes (e.g., *BCL7A*, *PAX5*, *CD79A*) were downregulated with age only in men (**Figs. 2e, S3d, S3e**), which might be linked to changes in cell compositions (**Fig. 1d**). Notably, aging-related transcriptomic changes correlated positively with aging-related epigenomic changes both in men (r=0.31, p<10-4, **Fig. S3g**, right panel) and in women (r=0.21, p<10-4, **Fig. S3g**, left panel). Module/pathway enrichment analyses of differential genes confirmed the upregulation of genes associated to cytotoxic cells and inflammation in both sexes (e.g., *GZMB*, *PRF1*, *NKG7* in women) (**Fig. S3f**) and downregulation of genes associated to T cells (e.g., *LEF1*, *TCF7*, *CCR7* in both sexes) (**Table S8**). These data and analyses demonstrate that, although transcriptomes are remodeled less significantly with age compared to epigenomes, age-related changes in both modalities correlate significantly. Together we detected an age-related shift in PBMC epigenomes/transcriptomes from adaptive to innate immunity in both sexes, though more pronounced in men.

Age-related changes in monocyte- and B cell-associated loci differ between sexes

Age-related remodeling (i.e., fold changes from differential analyses) detected in ATAC-seq (**Fig. 3a**, r=0.435, p<0.001) and RNA-seq data (**Fig. 3b**, r=0.484, p<0.001) positively correlated between sexes. However, enrichment analyses of peaks/genes using Roadmap[18] and scRNA-seq data revealed that the similarity between sexes depends on the cell type (**Figs 3c, 3d**). For example, age-related changes in naïve T cells were highly correlated between sexes both in transcriptomic (r=0.698 in **Fig. 3d**) and epigenomic data (r=0.705 in **Fig. 3c** for naïve T cells**, Fig. S4a** for T cell subsets), where these peaks/genes lost accessibility and expression in both sexes, potentially due to the loss of naïve T cells with age (**Figs. S1d, S1e**). These included age-related changes for important molecules shared between sexes including the receptor gene *IL7R* - which we previously associated to aging (**Fig. 2d**)[5] - chemokine receptor *CCR7*, co-receptor *CD8A*, and transcription factors *TCF7* and *LEF1* (**Table S6**). Gene expression levels of these molecules also decreased with age in both sexes (**Figs. 2d, 3e**). Similarly, age-related changes in cytotoxic cells were highly correlated between sexes (RNA-seq: r=0.621 for NK cells, r=0.772 for cytotoxicity module; ATAC-seq: r=0.521 for NK cells r=0.675 for cytotoxicity module) (**Figs. 3c, 3d, S4b, S4c**). The activity of cytotoxic molecules increased with age (chromatin opening and

higher expression) in both sexes, including granzyme B (*GZMB*) and perforin (*PRF1*), which work together to kill target cells, and *KLRF1*, which is selectively expressed in NK cells[21] in comparison to cytotoxic T cells (CTLs) (**Fig. 3e**). These results combined with our previous study[5] suggest that both CTLs and NK cells contribute to the increased cytotoxicity observed with aging in both sexes. In contrast, age-related remodeling of peaks/genes associated to monocytes and B cells showed the lowest correlation between sexes (**Figs. 3c, 3d, S4b, S4c**). In monocytes, we observed that the majority of peaks/genes were activated with age in both sexes; however, the magnitude of activation was higher in men (**Fig. 2c**), which reduced the correlations between sexes (r=0.267 for RNA-seq, 0.171 for ATAC-seq) (**Figs. 3c, 3d**). These included pro-inflammatory cytokines (e.g., *IL18*, *IL1B*), as well as *S100A8/S100A9* that modulate inflammatory responses and serve as potential biomarkers of inflammation-related diseases[22]. In B cells, the distinction between sexes stemmed from the male-specific downregulation/chromatin closing of B-cell specific loci/genes (r=0.195 for RNA-seq, 0.017 for ATAC-seq) (**Figs. 3c, 3d**), including the chemokine receptor *CXCR4* and B cell antigen receptor *CD79A* (**Fig. 3e, Table S6**).

Together, these data revealed that the degree of similarity between the aging signatures of men and women depends on the cell type. Loci associated with naïve T cells lost accessibility/expression with age in both sexes, whereas those associated with NK and memory CD8+ T cells gained accessibility/expression in both sexes. Gain of accessibility/expression for monocyte-specific loci was greater in men, which contributed to the sex-dimorphic aging patterns in PBMCs. B cell-specific loci lost activity/expression with age only in men, representing the most divergent aging pattern between sexes.

Chromatin accessibility and gene expression changes over adult lifespan

We uncovered chronological trends in epigenomic and transcriptomics maps over the entire adult lifespan using Autoregressive Integrated Moving Average (ARIMA)[23] models by testing for the presence of a significant temporal change for each peak/gene. First, we identified the best-fitting ARIMA model to each peak/gene as a function of age. Then, peaks/genes that displayed a chronological trend that is significantly different from random fluctuations were selected. These analyses uncovered 13,297 (17%) and 13,295 (17%) ATAC-seq peaks with a temporal trend in women and men, respectively. These peaks were then grouped into three major clusters based on the similarity of their genomic patterns (**Fig. 4a, Table S9**). Cluster 1 (F1 and M1 in **Fig. 4a**) included peaks losing accessibility with age, whereas clusters 2 and 3 included peaks gaining accessibility with age (F2/M2 and F3/M3 in **Fig. 4a**). In cluster 3, the gains occurred earlier (~10-20 years) than in cluster 2.

Enrichment analyses of temporal peaks using cell-specific loci/genes revealed that, in both sexes, cluster 1 was associated to T cell-related loci, particularly naïve T cells (**Figs. 4b, S5a**). Interestingly, cluster 1 was significantly enriched in B cell-specific regions only in men (**Fig. S5a**), reinforcing a male-specific decline in B cell functions with age. Cluster 2 was most significantly enriched in monocyte-specific regions in both sexes, albeit more significantly in men (**Figs. 4b, S5a**). Finally, cluster 3 was most significantly enriched in NK cell-specific regions in both sexes, again more significantly in men (**Figs. 4b, S5a**). Although less significant, we also detected female-specific enrichment of B cell-specific regions in clusters 2 and 3, contrasting the declines observed in men (**Figs. 2c, 4b**).

Application of ARIMA models to RNA-seq data revealed temporal transcriptomic patterns consistent with the epigenomic patterns. 1,068 and 1,471 genes had temporal trends across human lifespan respectively in women and men (**Fig. 4c, Table S9**). Consistent with the epigenomic trends, these genes grouped into three clusters in both men (M1-3) and women (F1-3) based on the similarity of temporal trends. Enrichment analyses using cell-specific gene sets[10] revealed shared changes between sexes including declining expression of naïve T cell genes and increasing expression of monocyte, NK, and effector T cell genes (**Figs. 4d, S5b**). Similar to the epigenomic trends, temporal genes of men and women differed for the B cell compartment, where we detected a male-specific decline in the expression of B and plasma cell-specific genes (cluster 1 in **Figs. 4d, S5b**) and a female-specific increase – albeit weaker – in the expression of plasma B cell-specific genes (clusters 2 and 3 in **Fig. 4d**). These data suggest that, other than in the B cell compartment, temporal epigenomic/transcriptomic trends are shared between men and women, which can be summarized as chromatin closing (declining expression) with age associated to T cells, especially naïve T cells, coupled with chromatin opening (increasing expression) associated to monocyte and NK cells.

PBMCs go through rapid epigenomic changes at two discrete periods during adult lifespan

To study whether temporal epigenomic changes are acquired gradually over lifespan or more rapidly at certain ages, we developed a method that can detect age brackets during which abrupt changes take place, referred to as breakpoints. Within each temporal cluster (**Fig. 4a**), for each time point, this method compares epigenomic profiles observed at ages immediately preceding and succeeding this age (e.g., 5 years before and after) and calculates a p-value for observed differences between the two windows. To ensure robustness to outlier samples, sample sparsity at certain ages, and fluctuations in temporal trends, we used a moving window approach with varying sizes that span 10 to 20 years (**Fig. S5c**). Finally, for each age, a combined p-value was calculated from different windows, where a smaller p-value for a given

age indicates that at that age the epigenomic maps change rapidly. Due to sample sparsity for RNA-seq data, these analyses were restricted to ATAC-seq samples.

These analyses revealed two periods in the human lifespan during which rapid epigenomic changes take place: i) a timepoint in the late thirties/early forties, and ii) a later timepoint after 65 years of age (**Figs. 4e, S5c**). In women, the earlier breakpoint was detected between ages 38 to 41 across three clusters (cluster F1:38-43, median 38; cluster F2: 41-46, median 41; cluster F3: 37-46, median 38) (**Fig. 4e**). In males, a comparable breakpoint was detected between ages 40 to 42 only across clusters 1 and 3 (cluster M1: 38-41, median 40; cluster M3: 38-42, median 42), with no significant breakpoint in this interval for cluster M2. Magnitude (based on the breakpoint p-values in **Fig. 4e**) and timing of the changes for this breakpoint were similar between men and women. When interpreted together with **Fig. 4a**, this time interval coincided with the start of aging-related changes in epigenomic profiles, i.e., the start of losses in chromatin accessibility in cluster 1 and gains in clusters 2 and 3. The later breakpoint was detected between ages 66 to 71 in women across three clusters (cluster F1: 63-70, median 66; cluster F2: 68-71, median 71; cluster F3: 65-69, median 68) (**Figs. 4e, S5c**). Interestingly, in men, this breakpoint was observed earlier in life between ages 62 and 64 in all three clusters (cluster M1: 61-63, median 62; cluster M2: 63-64, median 64; cluster M3: 62-64, median 63). Unlike the first breakpoint, the magnitude of changes for the second breakpoint was more pronounced in men than in women (e.g., -log P-value for cluster 2 was 197.27 in men and 124 in women, **Figs. 4e, S5c**), suggesting that the epigenomic remodeling at this breakpoint was more abrupt in men. Combined with **Fig. 4a**, this latter breakpoint coincided with ages during which epigenomic changes accelerated, such as a faster loss of chromatin accessibility in cluster 1 (i.e., associated with naïve T cells). In summary, breakpoint analysis revealed that, although aging-related changes accumulate gradually, there are at least two periods in the human lifespan during which the immune system undergoes more abrupt epigenomic changes. The first breakpoint manifests itself both in men and women in their late thirties and early forties, whereas the second breakpoint is observed later in life and affects men more strongly and earlier (early- to mid-sixties) than women (mid-sixties to early seventies). Interestingly, confidence intervals for both breakpoints overlapped across clusters (**Figs. 4e, S5c**), suggesting that even though different cell types go through distinct age-related changes, timing of these changes are harmonized across cell types suggesting that cellular interactions might modulate these changes.

Shared temporal genomic patterns between men and women

We detected 3,197 peaks and 180 genes with a temporal trend in both sexes, which are grouped into three clusters both in ATAC-seq (**Fig. 5a**) and RNA-seq data (**Fig. S6a**). Cluster 1 (**Figs. 5a, S6a**) captured a

downward trend consistent between sexes in both datasets and was mainly associated with naïve T cells (**Figs. 5b, S6b**). Similarly, cluster 3 (**Figs. 5a, S6a**) exhibited an upward trend with age consistent between sexes, and was most strongly associated with monocytes and NK cells (**Figs. 5b, S6b**), in agreement with previous results (**Figs. 4b, 4d**). Interestingly, cluster 2 (**Figs. 5a, S6a**) exhibited opposite temporal patterns between sexes, i.e., a downward trend in men and an upward trend in women and was associated to B cells (**Figs. 5b, 5c, S6b**).

Further inspection of these clusters identified temporal changes for functionally important immune molecules. Cluster 1 included genes required for T cell survival and development, including the co-stimulatory molecule *CD27* and transcription factor *TCF7*, which is a key TF in T cell development and can change chromatin accessibility levels[24] (**Table S9**). Expression of both of these molecules decreased with age, but the decrease was faster in men compared to women (**Fig. S6d**). On the other hand, cluster 2 exhibited contrasting temporal patterns between sexes and was associated to B cells, including plasma cells, in both ATAC-seq and RNA-seq data (**Figs. 5b, S6b**). These included *TCF4* (E2.2) - a member of the E proteins that control various aspects of B cell development[25] - whose expression levels increased in women and decreased in men with age (**Fig. S6d**). Similarly, the expression levels of *ORAI2* -a member of the B cell receptor signaling pathway - increased with age in women and decreased in men (**Fig. S6d**). Changes in cluster 3 included increases in the expression of *JAG2* in both sexes, which is specifically expressed in NK cells[10] and plays critical roles in DC-mediated NK cell cytotoxicity[26] (**Fig. S6d**).

To uncover potential regulators of chromatin accessibility changes with age, we identified TF motifs enriched in loci with a temporal trend using 1,388 known motifs for 681 TFs, which were grouped into 278 motif families based on their sequence similarity. 50 of these motif families were significantly enriched across three clusters in **Fig. 5a**. These included families that were enriched across all three clusters (e.g. a bHLH family including motifs for TCF3, TCF4, and TAL1) as well as TFs that are enriched in a single cluster (**Fig. 5d**, **Table S10,** see **Fig. S6e** for separate analyses in men and women). TFs that are associated to naïve T cells[10] were enriched in cluster 1 including NPAS2, TCF7, SOX12, and FOXO1. Among these TCF7 is a potential 'pioneer factor' in T cells, hence can impact the chromatin accessibility levels[24]. Expression levels of these TFs also decreased with age (**Fig. 5e**). Cluster 3 was enriched for motifs of MAFB, CEBPA, CREB5, and NFE2, which are highly expressed in monocytes[10] and had increased expression levels with age in PBMCs (**Fig. 5f**). TF enrichments for cluster 2 were not as significant due to the small number of peaks in this cluster. In summary, combined analyses of temporal trends in men/women uncovered changes shared between sexes: i) downward trends in epigenomes/transcriptomes associated with naïve T cell genes and TFs, including the pioneer factor

TCF7; ii) gains associated with genes and TFs active in monocytes and cytotoxic cells. These analyses further highlighted the stark differences between sexes in terms of the aging of the B cell compartment.

PBMCs of men and women diverge with age

We compared ATAC-seq and RNA-seq maps of men and women at different age groups to systematically describe sex-bias in human PBMCs. These comparisons were restricted to autosomal chromosomes since differences in sex chromosomes were expected at all ages. In young and middle-aged subjects, very few differences were detected between sexes in ATAC-seq (FDR 5%) and RNA-seq data (FDR 10%) (**Figs. 6a, 6b**). Interestingly, these differences increased after the age of 65, where 1011 differential peaks and 548 differential genes were detected between men and women using the same significance cut-offs (**Figs. 6a, 6b**). Notably, functional annotations of these differential regions were conserved between the two assays (**Figs. 6c**), using cell-specific marker genes and immune modules[20]. We detected a bias toward the activity of myeloid- and particularly monocyte-specific loci in older men relative to older women (**Figs. 6c, S7a, Table S11**). In contrast, we detected a bias towards increased accessibility/expression of lymphoid cell (B and T) specific loci in older women relative to older men (**Figs. 6c, S7a**, **Table S11**). These trends were confirmed using cell-specific loci from the Roadmap data[18] (**Figs. S7b, S7c**), where male-biased peaks were enriched in monocyte-specific loci and female-biased peaks were enriched in B and T cell-specific loci, including important signaling molecules such as *JAK3* and *STAT5B* (**Table S11**). Furthermore, loci/genes associated to the IL7 signaling pathway and other B/T signaling pathways were more active in PBMCs of older women compared to older men (**Fig. 6d, Tables S12, S13**). Given that genes in this pathway lose activity with age in both sexes (**Fig. 6d,** right table), the observed difference between older subjects suggest that the age-related declines are greater in men. In contrast, immune module enrichments of sex-biased loci uncovered that older men have higher inflammation compared to older women (**Fig. 6d, Tables S12, S13**), including the pro-inflammatory cytokine *IL18*. We detected increased chromatin accessibility for inflammation related genes/loci in both sexes (**Fig. 6d,** right table), suggesting that although both men and women both experience increased inflammation with age, the increase in men is greater. In agreement with these observations, re-analyses of serum protein measurements from the 500 Human Functional Genomics (500FG) consortium[11] cohort (n=267) revealed that older men have higher levels of pro-inflammatory proteins (IL18BP, IL18, IL1RA, IL6) compared to older women (**Fig. 6e**). Interestingly, levels of IL18BP and IL6 increased with age in both sexes, however, the age-related increase was greater in men which led to the significant differences between sexes after the age of 65. On the other hand, serum IL1RA levels increased specifically in men with age, also leading to significant differences (p=0.0065) between men and women after 65 years old (**Fig. 6e**).

These data suggest that older men have more active genomes associated to innate immunity, whereas older women have more active genomes associated to adaptive immunity. The male bias in innate cells partially stems from the elevated activation of monocyte and inflammation related genes/loci with age in men (**Figs. 2c, S3c**). For example, 15 times more monocyte-specific loci were activated in men with age: 960 peaks in men vs. 64 peaks in women. (**Fig. S2e**). However, we did not detect significant differences between men and women in terms of $CD14^+$ and $CD16^+$ monocyte cell numbers (absolute counts and frequencies) when we reanalyzed flow cytometry data from Milieu Intérieur Consortium[12] (n=892) (**Fig. S7d**) or in our flow cytometry data (**Fig. 1d**). Interestingly, the number of $CD16^+$ monocytes increased with age in both sexes (**Fig. S7e**), however, this increase was comparable between older men and older women and hence did not lead to a significant sex bias in older individuals in terms of their $CD16^+$ monocyte counts (**Figs. S7d, S7e**). On the other hand, the female-bias observed in the adaptive immunity, particularly in B cells, originated from a male-specific decline in the activity in B cells (**Figs. 2c, 4d**). Flow cytometry data suggest that this decline likely stems from the male-specific loss of B cells after 65 years of age (**Fig. 1d**), which was also observed in the Milieu Intérieur cohort in the numbers of different B cell subsets (i.e., naïve, transitional, founder) (**Figs. S7d, S7e**).

Discussion

Despite well-characterized sexual dimorphism in immune responses, disease susceptibility, and lifespan, it is unclear whether aging differentially affects peripheral blood cells in men and women, broadly and involving specific subpopulations. To fill this gap, we profiled chromatin accessibility (ATAC-seq), gene expression (RNA-seq), and cell composition (flow cytometry) profiles of PBMCs from a cohort of 194 carefully age-matched healthy adults representing the entire human lifespan. Using novel systems immunology pipelines, we discovered a genomic signature of aging that is shared between sexes, which is composed of 1) declines in T cell functions, 2) increases in cytotoxic (NK, memory CD8+ T) and monocyte cell functions with age. This common signature corresponds to the two hallmarks of immune system aging: immune-senescence and inflamm-aging[14]. We noted that, despite these similarities, male immune system goes through greater changes that are not attributable to clinical or cohort differences. Most notably, we detected 15 times more monocyte-specific loci to be activated in men compared to women. Previously, it has been reported from whole blood samples that the DNA methylome of men ages faster compared to women[27]. Here, we uncovered an accelerated aging phenotype for men in chromatin accessibility maps and uncovered which cell types, cellular functions, and molecules differentially age between men and women. In addition to this common signature, our data revealed for the first time that aging has opposing effects on the B cells of men and women, where B cell-specific loci/genes were

modestly activated in women but significantly inactivated in men, potentially linked to sex-differences in auto-immunity and humoral responses.

Our study is unique in its inclusion of data from middle-aged individuals to capture chronological changes and the timing of these changes, an approach that is essential in distinguishing changes attributable to aging from those resulting from maturation[28]. We captured correlated chronological patterns in chromatin accessibility and gene expression maps, including upward trends (i.e., increasing accessibility/expression with age) associated with cytotoxic cells and monocytes, and downward trends associated with T cells in both sexes. Combined analyses of male/female temporal patterns further highlighted the differential aging of the B cell-related loci. Breakpoint analyses uncovered that although aging-related changes accumulate gradually throughout adult life, there are two periods in the human lifespan during which the immune system undergoes abrupt epigenomic changes. The first breakpoint was around the late thirties in both sexes, whereas the second breakpoint was detected earlier in men (mid-sixties) compared to women (early seventies). Interestingly, this difference between sexes (5-6 years) is comparable to the difference in their life expectancy: 76.9 for men and 81.6 for women according to World Health Organization 2015 records for USA[29]. In both sexes, the second breakpoint was associated with accelerated epigenomic changes and occurred ~12-15 years prior to the end of the average lifespan. Our findings regarding the timing of age-related changes are novel and can be essential while making decisions regarding when to start clinical interventions/therapies.

Detailed comparison between sexes at different age groups uncovered that PBMCs of men and women significantly differed after the age of 65, contrary to expectations due to the decline in sex hormones. Annotation of sex-biased loci/genes revealed that older women have more genomic activity associated to adaptive cells (B/T cells), whereas older men have more genomic activity associated to innate cells, particularly monocytes and inflammation. Some of these genomic differences, but not all, could be attributable to changes in cell compositions, e.g., the decline of B cell frequencies exclusively in older men (**Fig. 1d**), which is confirmed in a second independent cohort[12] (**Fig. S7d**) and a previous study conducted in a Japanese cohort[30]. This concordance across cohorts suggests that sex-specific aging signatures described here might be conserved across ethnicities/populations, which needs to be further investigated in the future. Increase in monocyte associated loci/genes was associated with inflammatory pathways/genes and was more significant in men, suggesting an accelerated inflamm-aging signature for men. This signature was confirmed by an independent cohort[11] that showed that older men have higher levels of pro-inflammatory cytokines in their serum compared to older women (e.g., IL1RA, IL6, IL18) (**Fig. 6e**). Interestingly, neither in our data nor in data from a bigger cohort[12], could we detect significant

differences between older men and older women in terms of $CD14^+$ and $CD16^+$ monocyte cell numbers (absolute counts and frequencies) (**Figs. S7e, S7e**). Therefore, age-related activation of monocytes and differences between the sexes in the rate of activation likely stems from cell-intrinsic changes. It is currently unclear why men experience greater inflammation with age. Future studies are needed to explore potential reasons, including the role of infections, sex hormones, and differential activation of transposable elements[31].

By following a systems immunology approach in human PBMCs, this study uncovered which cell types and which immune functions are differentially affected with aging between men and women. Future studies are needed to more precisely describe these differences at single cell resolution and in sorted cells and to establish the functional implications of these sex differences. Moreover, future studies are needed to explore the potential of the molecules identified in this study (i.e., *IL7R*, *LEF1*, TCF7, *STAT5B*, *IL8*, *IL18*) as biomarkers of immune system aging in men and women and their role in contributing to sex differences in immunosenescence and inflamm-aging. Taken together, these findings indicate that sex plays a critical role in human immune system aging and should be taken into consideration while searching for molecular targets and time frames for interventions/therapies to delay aging and age-related diseases.

Author contributions

D.U., G.A.K. and J.B designed the research. G.A.K coordinated the clinical sample collection. C.C., R.M., R.R., performed the experiments. E.M pre-processed the sequencing data. E.M, D.U., DJM, and D.N. analyzed the data. E.M., D.U. wrote the paper. DJM implemented the R Shiny application. All authors revised the manuscript and helped with data interpretation.

Acknowledgements

We thank Taneli Helenius for aid in scientific writing, research staff in the UConn Center on Aging for their help in recruitment and sample collection, JAX genomic technologies for their help with generating the sequencing data, and JAX Research IT for the support with building and maintaining the R Shiny application. We thank members of Ucar, Stitzel, Bachereau labs, Michael Stitzel, Karolina Palucka, Virginia Pascual, Derya Unutmaz for critical feedback during the progress of the study. We thank Yuqi Zhao for his help with data upload. This study was made possible by generous financial support of the National Institute of General Medical Sciences (NIGMS) under award number GM124922 (to DU) and National Institutes of Health

(NIH) grants R01 AG048023, P01 AG021600, U19AI089987 (to JB). Opinions, interpretations, conclusions, and recommendations are solely the responsibility of the authors and do not necessarily represent the official views of the National Institutes of Health (NIH). G.A.K is supported by the Travelers Chair in Geriatrics and Gerontology.

Data and code availability

The data generated as part of this study is controlled access. A subset of the ATAC-seq and RNA-seq samples used in these analyses was made public through EGA (Study ID: EGAS00001002605). Rest of the ATAC-seq and RNA-seq samples will be deposited to dbGAP upon publication. The code used for all data analyses will be made public through our GitHub page (https://github.com/UcarLab) upon publication. The R Shiny app is shared at a temporary URL during revisions (https://shinyapps.jax.org/44c0a53ebb13f7fd5e2ddbced1a37f51/). Upon publication, it will be shared publicly and will be maintained regularly.

Main figure legends

Figure 1. Age is the main driver of variation in PBMC ATAC-seq/RNA-seq data. (**a**) Schematic summary of study design: PBMCs were isolated from blood samples of 194 healthy community-dwelling individuals (ages 22-93), from which ATAC-seq, RNA-seq and flow-cytometry data are generated. (**b**) Principal component 1 scores (PC1) were calculated for each individual from ATAC-seq (left) and RNA-seq (right) principal component analyses (PCA) results. Marker genes are selected using PC1 scores that are >= 25th percentile: top (positive) and bottom (negative). PC1 scores from ATAC-seq and RNA-seq data increased with increasing age. Furthermore, we detected differences in PC1 scores of sexes in older subjects, where older men had higher scores than older women. (**c**) Functional enrichment of PC1-related genes based on immune modules[20]. Note that myeloid/inflammation related genes were associated with high and positive scores, whereas adaptive immunity/lymphoid related genes were associated with high negative PC1 scores. These enrichments align well with an age-related increase in the myeloid lineage and inflammation, and an age-related decline in naïve T cell activity. Hypergeometric test was used to calculate enrichment p values. (**d**) Flow cytometry data from 130 individuals that reflect proportions of major cell types within PBMCs. Subjects were stratified based on age group and sex: Young: 22-40, Middle-aged: 41-64, Older: 65+ years old. Wilcoxon signed rank test was used to compare values from female and male subjects, and older and young individuals. Note that T cell proportions decline with age in both sexes, whereas the decline in B cell proportions is specific to older men.

Figure 2. **Shared and sex-specific chromatin accessibility signatures of aging.** (**a**) MA plot representing log2 fold change (older-young) versus average read count for ATAC-seq peaks in women (left) and men (right). Peaks differentially opening (closing) with age are represented in orange (purple). Note that age has a stronger effect on male epigenomes, evinced both in the magnitude of fold change values and the number of differential peaks. Differential accessibility of ATAC-seq peaks was tested using a generalized linear model based on read counts, with significance assessed at a 5% FDR threshold, after using Benjamini-Hochberg P-value adjustment. (**b**) Functional state annotations for differentially opening/closing peaks in men and women using chromHMM states in PBMCs and immune cell subsets. Closing peaks tend to be enhancers/promoters across all cell types, whereas opening peaks tend to be enhancers in monocytes and NK cells. (**c**) Distribution of differentially accessible (DA) peaks among cell-specific loci based on chromHMM states. Loci specific to innate cells (i.e., monocytes and NK cells) are enriched in opening peaks, whereas loci specific to T cells are enriched in closing peaks. Interestingly, B cell specific loci are more likely to be a opening peak in women and closing peak in men. Note that, a much larger number of monocyte-specific (CD14^{+}) loci are among opening peaks in men than in women. (**d**) Left: Average chromatin accessibility profiles (grouped by age and sex) around the *IL7R* locus in women (top) and men (bottom). In both sexes, this locus

is associated with chromatin closing with age. Right: Normalized chromatin accessibility (average of three peaks shown in the figure) and gene expression levels for *IL7R* in young and older women (top) and men (bottom). In both sexes, chromatin accessibility and gene expression levels decline for this molecule with age. The decline is much more significant in men. (**e**) Enrichment of differentially expressed (DE) genes using cell-specific gene sets from scRNA-seq data. Enrichment p values are calculated using hypergeometric test. Note the activation of gene expression programs for innate cells (NK, monocytes) and inactivation for T cell programs in both sexes. In agreement with ATAC-seq, B-cell specific genes were downregulated with age specifically in men. (**f**) Average normalized expression levels of T cell-specific genes grouped by age group and sex. Note the decline in both sexes. Box plots on the top summarizes the data from all genes represented in the heatmap.

Figure 3. Aging-related changes in monocyte- and B cell-associated loci differ between sexes. Correlation of age-related ATAC-seq (**a**) and RNA-seq (**b**) remodeling between women and men PBMCs. Note the overall positive and strong correlation. Gene names are color coded according to their cell-specific activity in single-cell RNAseq data (purple: T cells, green: B cells, pink: NK cells, yellow: monocytes). Colors on data points represent the density of data points. (**c**) Correlation between sexes for age-related ATAC-seq remodeling stratified by cell-specific loci from chromHMM annotations. Note that the highest correlation is observed in naïve T cells, which is associated with negative fold changes (i.e., loss in chromatin accessibility with age) in both sexes. Chromatin remodeling correlates the least between sexes for B and monocyte-specific loci. (**d**) Correlation between sexes for age-related RNA-seq remodeling stratified by cell-specific genes from scRNA-seq data. Note that the highest correlation is observed in naïve T cells, which is associated with negative fold changes (i.e., downregulation with age) in both sexes. On the other hand, NK cells are highly correlated between sexes and associated with increased expression with age in both sexes. In agreement with ATAC-seq data, gene expression remodeling correlates the least between sexes for B and monocyte-specific genes. Values at the top left corner represent the correlation coefficient between sexes only for the genes/loci associated to that cell type. (**e**) Normalized expression and accessibility levels for important molecules associated to T, cytotoxic, and B cells. MA = middle-aged.

Figure 4. Chromatin accessibility and gene expression changes over human adult lifespan. (**a**) Heatmap of ATAC-seq data (fitted values from ARIMA models) with a significant chronological trend in women (left, n=13,297) and men (right, n=13,295). Values represent z-score normalized accessibility values relative to the row mean. K-means clustering was used to group these peaks into three clusters in men and women (M1/F1, M2/F2, M3/F3). Color bar on the top represents discrete age groupings as defined in this study (young, middle-aged, older). Rows are annotated according to their position relative to the nearest TSS: proximal if within <1kbp distance, distal if distance is greater than 1kbp. (**b**) ChromHMM state annotations of temporal peaks in women (F1-F3) and men (M1-M3). Colors represent hypergeometric enrichment test P-values. (**c**) Heatmap of ARIMA-fitted expression values for genes with a significant chronological trend in women (left, n=1,068) and men (right, n=1,471). Three clusters per sex are determined using k-means clustering: F1-3 and M1-3. Values represent z-score normalized gene expression values relative to the row mean. (**d**) Annotation of temporal gene clusters using cell-specific gene sets derived from scRNA-seq data. Colors represent hypergeometric enrichment test P-values. Grey cells in plot indicate that there were insufficient genes in the gene sets to run an enrichment test. (**e**) P-values from breakpoint analysis for each cluster for women (top) and men (bottom). Note that there are two age brackets where epigenomic changes take place abruptly both in men and women. Points and vertical lines mark median age estimates for a breakpoint integrated over multiple scales (see Methods and **Figure S5c** for details).

Figure 5. Combined analyses of temporal patterns in men and women uncovered sex-specific patterns. (a) Heatmap of ATAC-seq peaks (fitted values from ARIMA models) with a chronological trend in both women and men (N=3,197). Values represent z-score normalized accessibility values relative to the row mean. K-means clustering was used to group these peaks into three clusters (C1-C3) using concatenated data from men and women. Color bar on the top represents discrete age groupings as defined in this study (young, middle-aged, older). Rows are annotated according to their position relative to the nearest TSS: proximal if within <1kbp distance, distal if distance is greater than 1kbp. (**b-c**) Annotations of shared temporal peaks using chromHMM states (**b**) and gene sets from DICE database[10] (**c**). Colors represent hypergeometric enrichment test P-values. The enrichment pattern strongly associates cluster C1 to T cells, suggesting a delayed loss of accessibility in women relative to men; C2 to $CD19^+$ cells, suggesting the presence of $CD19^+$ specific loci with opposing temporal behavior in men and women; and C3 to monocytes and NK cells. Grey cells in plot indicate that there were insufficient genes in the gene sets to run an enrichment test. (**d**) Transcription factor (TF) motif enrichment results for each temporal cluster (C1-C3), relative to the other two clusters. Motif enrichment analyses carried out on 1,388 PWMs, grouped into families based on the

sequence similarity, and most significant p-value for each family is represented here. (**e-f**) Expression levels of TFs associated to cluster 1 (C1) and cluster 3 (C3) grouped by age group and sex. Cluster 2 (C2) is omitted since it lacks sufficient number of peaks to allow an enrichment test.

Figure 6. Epigenomic and transcriptomic differences between men and women at different ages. (**a**) MA plot representing log2 fold change (male-female) versus average read count for ATAC-seq data at three age groups using only peaks on autosomal chromosomes. Epigenomic differences between sexes increase with age. Peaks more open in women (men) are represented in red (blue). (**b**) MA plot representing log2 fold change (male-female) versus average read count for RNA-seq data at three age groups using only genes on autosomal chromosomes. Transcriptomic differences between sexes increase with age. Genes more expressed in women (men) are represented in red (blue). (**c**) Enrichment of sex-biased peaks/genes in older individuals using cell-specific gene sets obtained from scRNA-seq data. Note the male bias toward increased accessibility/expression for monocytes and DCs and the female bias toward increased accessibility/expression for T and B cells. P-values are based on hypergeometric enrichment tests. Numbers on barplots represent the number of gene hits for each gene set. (**d**) Left: Selected pathways/module enrichments for male-biased and female-biased genes/loci. The complete list of enrichments is presented in Tables S12, S13. * represents annotations obtained from ATAC-seq data analyses. Right: Arrows indicating whether the same pathway/module has been significantly associated with age-related changes. Significant enrichments (FDR 5%) and their directions are represented with arrows. Red arrows for women, blue arrows for men. NS = not significant. The complete list of enrichments is presented in Tables S6, S8. (**e**) ELISA data from 500 Functional Genomics (500FG) project to measure serum levels of pro-inflammatory cytokines (n=267). Protein expression levels are compared between sexes and between young and older individuals. P-values were calculated using Wilcoxon signed rank test.

Supplementary figure legends

Figure S1. **Age is the main driver of variation in PBMC ATAC-seq/RNA-seq data.** Principal component analyses for all (**a**) RNA-seq (n=74) and (**b**) ATAC-seq samples (n=100). PC1 explains 18.6% of variation in RNA-seq data, whereas it explains 15% of variation in ATAC-seq data. (**c**) Functional enrichment of PC1-related genes using gene sets obtained from single-cell RNA-seq data in PBMCs. Marker genes are selected using PC1 scores that are >= 25th percentile: top (positive) and bottom (negative). Genes with high and positive scores were enriched in myeloid cells (monocytes, DCs), whereas genes with high and negative scores were associated to adaptive cells, particularly naïve T cells. These enrichments align well with age-related increase in myeloid lineage and age-related decline in naïve T cell activity. Hypergeometric test is used to calculate enrichment p values. (**d-e**) Flow cytometry data from 81 individuals that reflect proportions of $CD4^+$ (**d**) and $CD8^+$ (**e**) T cell subsets within PBMCs. Subjects are stratified based on age groups and sex: Young: 22-40, Older: 65+ years old. Wilcoxon signed rank test is used to compare values from female and male subjects, old and young individuals. Note that naïve $CD4^+$ and $CD8^+$ T cell proportions decline significantly with age in both sexes. (**f**) Significance values from generalized linear models (GLM) to establish the association between PBMC cell composition data with age group, sex, and their interaction (age*sex). Darker colors indicate stronger association. Age is most strongly associated with the variation in naïve T cell proportions, whereas sex, age*sex is most strongly associated with the variation in B cell proportions. (**g**) Top: Distribution of subjects by age and sex, showing a comparable spread of ages between sexes and among decades. Bottom: Distribution of Rockwood frailty index values[33] stratified by age groups and sexes. No significant difference detected between men and women at all three age groups. Note that the frailty index values increase with age, more so in women with none of the individuals having a Frailty Index value greater than 0.25. Most subjects were non-frail (Frailty index (FI): 0-0.1), a few were prefrail (FI >0.1-0.21) but regardless the frailty did not influence the observed genomic changes.

Figure S2. Shared and sex-specific chromatin accessibility signatures of aging. (**a**) Overlap between differentially accessible (DA) peaks (top) and genes associated to DA peaks (bottom) in women and men. Closing peaks overlap more between men and women. Note that the overlap is statistically significant for both opening and closing peaks based on Fisher's exact test for p-value calculations. (**b**) Distribution of cell-specific and cell-agnostic loci among DA peaks based on chromHMM states in PBMCs and immune cell subsets. Cell-specific regions are notably more common among opening peaks. (**c**) Number of cell-specific loci among closing/opening peaks in men and women. T and B cell-specific peaks are more prevalent among closing peaks, whereas NK and $CD14^+$ monocyte specific peaks are more prevalent among opening peaks. (**d**) Fold change (old-young) distributions for chromatin accessibility levels at cell-specific loci. Biggest decrease is observed in naïve $CD8^+$ T cell-specific loci in both men and women. Biggest increase is observed at $CD14^+$ monocyte specific loci. The increase was much

stronger in men. B cells specific loci on the average gain accessibility in women and lose accessibility in men with age. (**e**) Enrichment of cell-specific loci among DA peaks. Enrichment p values are calculated using hypergeometric test. Note the activation of innate cells (NK and monocytes) and inactivation of T cells with age. The enrichment p-values were more significant in men compared to women. B cell-specific regions were enriched for closing peaks in men and for opening peaks in women. Grayed out circles are non-significant at a 5% FDR; numbers on circles represent the number of peaks in each category.

Figure S3. Shared and sex-specific gene expression signatures of immune system aging. (**a**) MA plot representing log2 fold change (older-young) versus average read count for RNA-seq data in women (left) and men (right). Differentially upregulated (downregulated) genes with age are represented in orange (purple). Differential gene expression was tested using a generalized linear model based on read counts, with significance assessed at a 10% FDR threshold, after using Benjamini-Hochberg P-value adjustment. (**b**) Overlap between differentially expressed (DE) genes in women and men. Note that despite sex differences, overlaps are statistically significant based on Fisher's exact test for p-value calculations. (**c**) Distribution of fold changes for gene expression levels of all cell-specific genes. Positive (negative) fold changes represent upregulation (downregulation) with age. $CD14^+$ monocyte-specific genes are associated with positive fold change in both sexes, higher in men. B cell-specific genes are associated with negative fold changes only in men. (**d**) Enrichment of DE genes using cell-specific gene sets from the DICE database[10]. Naïve T cell genes are enriched in downregulated genes, NK cell genes are enriched in upregulated genes. B cell-specific genes are enriched in downregulated genes only in men. Enrichment p values were calculated using hypergeometric test. (**e**) Average normalized expression levels of B cell specific genes grouped by age group and sex. Box plots on the top summarizes the data from all genes represented in the heatmap. (**f**) Average normalized expression levels of genes in the cytotoxic module grouped by age group and sex. Note the increase in cytotoxic molecules in both sexes. Box plots on the top summarize the data from all genes represented in the heatmap. (**g**) Correlation of age-related chromatin accessibility and gene expression changes based on chromatin accessibility at promoters in women (left) and in men (right). Color schema represent the density of points. Note that age-reated remodeling ATAC-seq and RNA-seq data correlates positively and significantly in both sexes. R represents the correlation coefficient.

Figure S4. Aging-related changes in monocyte- and B cell-associated loci differ between sexes. (a) Correlation of age-related ATAC-seq changes stratified by T cell subset specific loci from chromHMM states. Values at the top left corner represents the correlation coefficient between sexes only for the genes/loci associated to that cell type. (**b-c**) Correlation of age-related RNA-seq (**b**) and ATAC-seq (**c**) changes stratified by immune modules[20]. Values at the top left corner represents the correlation coefficient between sexes only for the genes/loci associated to that cell type/module.

Figure S5. Chromatin accessibility and gene expression changes over human adult lifespan. (**a**) Annotations of temporal peaks using cell-specific expression (top) and chromatin states (bottom) in women (F1-F3) and in men (M1-M3). Colors represent hypergeometric enrichment test P-values. Single-cell RNA-seq-based enrichments based on nearest-gene annotations of temporal peaks. (**b**) Annotation of temporal genes using cell-specific gene sets from the DICE database[10]. (**c**) Detailed results from breakpoint analysis. Left: age range and median age of estimated breakpoints from each cluster in women (top) and men (bottom); Middle: -log (p-value) of smoothed multi-scale moving window tests. Age range estimates for each cluster are represented as thickened curves and wide vertical bars; Right: -log(p-value) of multi-scale analysis where each curve/color represents a distinct window span for the test, ranging from 10 to 20 years. Stronger evidence of a breakpoint emerges as the same age bracket is detected as significant at multiple window spans. C1, C2, C3 stands for cluster1-3.

Figure S6. Combined analyses of temporal patterns in men and women uncovered sex-specific patterns. (**a**) Heatmap of ARIMA-fitted expression values for genes with a significant chronological trend in both women and men (N=180). Values represent z score normalized gene expression values relative to the row mean. K-means clustering is used to group these peaks into three clusters (C1-C3) using concatenated data from men and women. Color bar on the top represents discrete age groupings as defined in this study (young, middle-aged, older). (**b**) Enrichment of cell-specific gene sets derived from scRNA-seq data among temporal clusters of OCRs, peaks are annotated to their nearest TSS. (**c**) Enrichment of cell-specific gene sets obtained from scRNA-seq among temporal and shared genes. Grey cells in plot indicate that there were insufficient genes in the gene sets to run an enrichment test. (**d**) Example temporal genes/peaks. (**e**) Transcription factor (TF) motif enrichment results for temporal peak clusters obtained separately from men and women. Peaks in each cluster is compared against the peaks in the other

two clusters. Motif enrichment analyses carried out based on 1,388 PWMs, grouped into families based on the sequence similarity, and most significant p-value for each family is represented here.

Figure S7. Epigenomic and transcriptomic differences between men and women at different ages. (**a**) Enrichment of sex-biased peaks/genes in older individuals using immune modules[20]. Note the male bias toward increased accessibility/expression for myeloid lineage and inflammation modules and the female bias toward T and B cell related modules. P-values are based on hypergeometric enrichment tests. Numbers on barplots represent the number of gene hits for each module. (**b**) Distribution of cell-specific loci among sex-biased peaks (left) and sex-biased genes (right). Note the enrichment of monocyte specific loci among male biased loci/genes. (**c**) Distribution of chromatin accessibility (left) and gene expression levels (right) in older men (blue) and older women (pink) for cell-specific genes. Stars next to the cell type name represent whether there is a significant difference between distributions in men and women. N represents the total number of cell-specific loci/genes used in each analysis. (**d**) Flow cytometry data from Milieu Intérieur Consortium[12] (n=892) re-analyzed using generalized linear models (GLMs) to associate cell counts or MFI values to sex. Rows represent the measurements that has been significantly associated to sex (FDR 5%). Values in heatmap represent the average value across individuals stratified based on sex and age group. Note the male-specific decline in different B cell populations after 65 years old, in agreement with our cohort. (**e**) Flow cytometry data from Milieu Intérieur Consortium[12] (n=892) re-analyzed using generalized linear models (GLMs) to associate cell counts or MFI values to age. Rows represent the measurements that has been significantly associated to age (FDR 5%). Values in heatmap represent the average value across individuals stratified based on sex and age group.

Supplementary table legends

Table S1. Detailed metadata on subjects, including types of data generated for each subject.
Table S2. Detailed information on ATAC-seq/RNA-seq samples including QC results.
Table S3. Principal component analyses (PCA) results from ATAC-seq/RNA-seq data.
Table S4. Flow cytometry data for proportions of sorted T cell and major cell populations (CD4+, CD8+, CD14+, CD19+) in PBMC samples.
Table S5. Differentially accessible ATAC-seq peaks between age groups.
Table S6. Annotation of DA peaks using chromHMM states, DICE and single-cell gene sets, immune modules, DICE and Wiki pathways.
Table S7. Differentially expressed (DE) genes between age groups.
Table S8. Annotation of DE peaks using DICE and single-cell gene sets, immune modules, and Wiki pathways.
Table S9. Expression/accessibility levels of temporal peaks/genes based on ARIMA models in men/women/shared.
Table S10. Summary of motif enrichment results for temporal peak clusters.
Table S11. Female versus male comparison results for ATAC-seq and RNA-seq data.
Table S12. Annotations for sex-biased transcripts using WikiPathways, immune modules, DICE and single cell gene sets.
Table S13. Annotations for sex-biased peaks using WikiPathways, immune modules, DICE and single cell gene sets.
Table S14. Gene sets used in enrichment analyses.

Materials and Methods

Human Subjects: All studies were conducted following approval by the Institutional Review Board of UConn Health Center (IRB Number: 14-194J-3). Following informed consent, blood samples were obtained from 194 healthy volunteers residing in the Greater Hartford, CT, USA region recruited by the UConn Center on Aging Recruitment and Community Outreach Research Core (http://health.uconn.edu/aging/research/research-cores/). For older adults 65 years and older, recruitment criteria were selected to identify individuals who are experiencing "usual healthy" aging and are thus representative of the average or typical normal health status of the local population within the corresponding age groups[5] Selecting this type of cohort is in keeping with the 2019 NIH Policy on Inclusion Across the Lifespan (NOT-98-024)34, increasing the generalizability of our studies and the likelihood that these findings can be translated to the general population[35]. Subjects were carefully screened in order to exclude potentially confounding diseases and medications, as well as frailty. Individuals who reported chronic or recent (i.e., within two weeks) infections were also excluded. Subjects were deemed ineligible if they reported a history of diseases such as congestive heart failure, ischemic heart disease, myocarditis, congenital abnormalities, Paget's disease, kidney disease, diabetes requiring insulin, chronic obstructive lung disease, emphysema, and

asthma. Subjects were also excluded if undergoing active cancer treatment, prednisone above 10 mg day, other immunosuppressive drugs, any medications for rheumatoid arthritis other than NSAIDs or if they had received antibiotics in the previous 6 months. Beyond these steps to exclude specific chronic conditions we also undertook further additional efforts to exclude older adults with any significant frailty. Since declines in self-reported physical performance are highly predictive of frailty, subsequent disability and mortality[36], all subjects were also questioned as to their ability to walk ¼ mile (or 2-3 city blocks). For those who self-reported an inability to walk ¼ mile[36], the "Timed Up and Go" (TUG) test was performed and measured as the time taken to stand up from the sitting position, walk 10 feet and return to sitting in the chair[37]. Scoring TUG > 10 sec was considered an indication of increased frailty and resulted in exclusion from the study[38]. Information on medications in **Table S1** illustrates that as expected medication usage did increase with age. Nevertheless, these medications all reflected their use for common and controlled chronic conditions unlikely to influence our findings such as hypertension, hyperlipidemia, hypothyroidism, degenerative joint disease, seasonal allergies, headaches, atrial fibrillation, depression, anxiety, or ADHD (attention deficit hyperactivity disorder). Finally, smoking history data are not typically collected in these studies –including ours- since smoking is a rare habit among older adults.

Flow cytometry data generation and analyses: PBMCs were isolated from fresh whole blood using Ficoll-Paque Plus (GE) density gradient centrifugation. For the analysis of the frequencies of Naïve T cells ($CD45RA^{+}CCR7^{+}$), Central Memory T cells (CM; $CD45RA^{-}CCR7^{+}$), Effector Memory T cells (EM; $CD45RA^{-}CCR7^{-}$), and Effector Memory RA (EMRA; $CD45RA^{+}CCR7^{-}$), B cells and Monocytes, PBMCs were stained with fluorochrome-labeled antibodies specific for CD3 (UCHT1), CD4 (RPA-T4), CD8 (SCF121Thy2D3), CD45RA (HI100), CD19 (HIB19), CD14 (MSE2), CCR7 (150503), and CD127 (HIL-7R-M21). The stained cells were acquired with BD Fortessa and analyzed with FlowJo software (TreeStar). Flow data is analyzed using Generalized Linear models (GLM) to quantify the association between cell proportions and age, sex, and their interaction (age and sex). For the analyses of major cell populations, we used age (continuous variable) as a covariate, whereas for T cell subsets we used age group (old vs. young) as a variable.

ATAC-seq library generation and pre-processing: ATAC-seq was performed as previously described[39]. Fifty thousand unfixed nuclei were tagged using Tn5 transposase (Illumina, Nextera DNA sample prep kit) for 30 min at 37°C and the resulting library fragments were purified using Qiagen MinElute kit (Qiagen). Libraries were amplified by 10-12 PCR cycles, purified using a Qiagen PCR cleanup kit (Qiagen), and finally sequenced on an Illumina HiSeq 2500 with a minimum read length of 75 bp to a minimum depth of 30 million reads per sample. At least two technical replicates (average = 2.4 replicates) were processed per biological sample. **Table S2** summarizes the depth, peak number, and fragments in reads (FrIP) scores for ATAC-seq samples. ATAC-seq sequences were quality-filtered using trimmomatic[40], and trimmed reads were mapped to the GRCh37 (hg19) human reference sequence using bwa-mem[41]. After alignment, technical replicates were merged and all further analyses were carried out on these merged data. For peak calling, MACS2[42] was used with no-model, 100bp shift, 200bp extension, and bampe option. Only peaks called with a peak score (q-value) of 1% or better were kept from each sample, and the selected peaks were merged into a consensus peak set using Bedtools multiinter tool[43]. Only peaks called on autosomal chromosomes were used in this study. We further filtered consensus peaks to avoid likely false positives by only including those peaks overlapping more than 20 short reads in at least one sample, and peaks for which the maximum read count did not exceed 500 counts per million (cpm) to account for regions that are potential artifacts. Finally, we excluded peaks overlapping ENCODE blacklisted regions downloaded from http://hgdownload.cse.ucsc.edu/goldenpath/hg19/encodeDCC/wgEncodeMapability/. An additional quality-control step was developed to filter out samples with a consistently poor signal, consisting of an algorithm to discover and characterize a series of relatively invariant benchmark peaks, defined as a set of peaks expected to be called in all samples. Samples that consistently miss calls for a significant portion of these benchmark peaks are flagged as having poor quality. A benchmark peak is defined based on three criteria, namely (1) that it remains approximately invariant between the two groups of interest (i.e., young and old samples), (2) that it captures a substantial number of reads, and (3) that it is called in most samples. For each peak, the absolute value of the log of the ratio of healthy old to healthy young mean normalized read counts (log fold change, logFC) was used to assess the first criteria, whereas the maximum read count over all samples (maxCt) is used to assess the second one. In this study, a peak was considered apt for benchmarking when (1) its absolute logFC was in the bottom quartile of the distribution over all peaks, (2) its maxCt was in the top decile of the distribution over all peaks, and (3) the peak was called in at least 90% of the samples. Using these parameters, 640 (out of 86,300) peaks were selected as benchmark; only samples for which at least 92.5% of these peaks were called were selected for analyses, which excluded 8 samples from further analyses. We examined the effects of each of these parameter choices and found that the same samples were

consistently chosen as poor quality for a range of values chosen to assess the benchmark criteria. After re-applying the peak selection criteria to the remaining 100 samples, we arrived at a peak count of 86,145 peaks. Prior to statistical analyses, ATAC-seq read counts were normalized to each sample's effective library size (i.e., the sum of reads overlapping peaks) using the trimmed mean of M-values normalization method (TMM)[44].

RNA-seq library generation and pre-processing: Total RNA was isolated from PBMCs using the Qiagen RNeasy (Qiagen) or Arcturus PicoPure (Life Technologies) kits following manufacturer's protocols. During RNA isolation, DNase I treatment was additionally performed using the RNase-free DNase set (Qiagen). RNA quality was checked using an Agilent 2100 Bioanalyzer instrument, together with the 2100 Expert software and Bioanalyzer RNA 6000 pico assay (Agilent Technologies). RNA quality was reported as a score from 1 to 10, samples falling below threshold of 8.0 being omitted from the study. cDNA libraries were prepared using either the TruSeq Stranded Total RNA LT Sample Prep Kit with Ribo-Zero Gold (Illumina) or KAPA Stranded mRNA-Seq Library Prep kit (KAPA Biosytems) according to the manufacturer's instructions using 100ng or 500ng of total RNA. Final libraries were analyzed on a Bioanalyzer DNA 1000 chip (Agilent Technologies). Paired-end sequencing (2x100bp) of stranded total RNA libraries was carried out in either Illumina NextSeq500 using v2 sequencing reagents or the HiSeq2500 using SBS v3 sequencing reagents. Quality control (QC) of the raw sequencing data was performed using the FASTQC tool, which computes read quality using summary of per-base quality defined using the probability of an incorrect base call[45]. According to our quality criteria, reads with more than 30% of their nucleotides with a Phred score under 30 are removed, whereas samples with more than 20% of such low-quality reads are dropped from analyses. Benchmarking is also applied on RNA-seq data using the same benchmark parameters as ATAC-seq, which resulted in 304 benchmark genes, none of the RNA-seq samples were dropped due to poor quality. Reads from samples that pass the quality criteria were quality-trimmed and filtered using trimmomatic[40]. High-quality reads were then used to estimate transcript abundance using RSEM[46]. Finally, to minimize the interference of non-messenger RNA in our data, estimate read counts were re-normalized to include only protein-coding genes. Table S2 summarizes the quality control measures for our PBMC RNA-seq samples.

Differential analysis: To identify differentially open chromatin regions from ATAC-seq and differentially expressed genes from RNA-seq data, the R package edgeR was used to fit a generalized linear model (GLM) to test for the effect of aging between healthy young and healthy old samples by sex, as well as the effect of sex by age group. In addition to sex and age group (old vs. young), our models included the base-2 log of effective library size to ensure peakwise normalization. We isolated a batch effect correlated to time period whereby samples were collected and libraries were prepared, and used ComBat to adjust the data for this effect. Finally, we used Surrogate Variable Analysis (SVA[47]) to capture unknown sources of variation (e.g., localized batch effects, subject-level heterogeneity, variation in library preparation techniques) statistically independent from age group assignments. SVA decomposes the variation that is not accounted for by known factors like age group or sex, into orthogonal vectors that can then be used as additional covariates when fitting a model to test for differential accessibility or expression. Using the built-in permutation-based procedure in the R package sva, we choose to retain one SV to include as covariate in the GLM model for PBMC ATAC-seq and none for RNA-seq data analyses[48]. GLM models where implemented using a negative binomial link function, including both genome-wide and peak-specific dispersion parameters, estimated using edgeR's "common," "trended," and "tagwise" dispersion components, calculated using a robust estimation option. Benjamini-Hochberg P-value correction was used to select differentially open peaks at a False Discovery Rate (FDR) of 5%. To generate a set of model-adjusted peak estimates of chromatin accessibility (i.e., batch-, and SV-adjusted) for downstream analyses and visualization, we used edgeR to fit a "null" model excluding the sex and age group factor, and then subtracted the resulting fitted values from this model from the original TMM-normalized reads.

Peak annotation and downstream analyses: Multiple data sources were used to annotate ATAC-seq peaks with regard to functional and positional information. HOMER[49] was used to annotate peaks as "promoter" (i.e., within 2 kb of known TSS), "intergenic", "intronic", and other positional categories. For functional annotation of peaks, we used a simplified scheme integrating public chromatin states calculated for major PBMC subpopulations with ChromHMM from Roadmap Epigenomics[18], Blueprint Epigenome, and a third reference data[50]: First, we intersected the chromHMM-generated states with our set of consensus peaks, and solved conflicting cases where multiple chromatin states overlap the same ATAC-seq peak so that each peak was assigned a single annotation, according to the following priority rules: if a peak overlaps both an active TSS and enhancer region, which state takes priority depends on whether the peak is proximal (i.e., within 1,000 bp of the nearest TSS), in which case it is annotated as a promoter, or distal (distance to nearest TSS greater than 1,000 bp), when it is annotated as an enhancer instead. For

all other states, rules apply as follows: Active Enhancer > Genic Enhancer > Bivalent TSS > Weak Enhancer > Bivalent Enhancer > PolyComb repressed > TSS Flanking > Transcription > ZNF Genes and repeats > Heterochromatin > Quiescent/Low signal. Then, to facilitate interpretation and visualization, we simplified the original sets of chromatin states to a scheme with 6 pooled meta-states, namely (1) TSS, collecting active, flanking, and bivalent TSS states; (2) Enhancer, pooling active, weak and bivalent enhancer states; (3) Repressed PolyComb, combining both weak and strong PolyComb states; (4) Transcription, including both weak and strong transcription states, (5) the quiescent chromHMM state; and (6) other states (ZNF, heterochromatin) combined together. To annotate peaks as cell-specific for a given subset obtained from one of the three datasets listed above, we determined for each peak whether it was annotated as an active promoter or an active enhancer in a single cell population or lineage, and in such cases labeled the peak accordingly as cell- or lineage specific. For example, if a peak is annotated as an active enhancer in both naïve and memory $CD4^+$ T cells but as another state (e.g., repressed) in every other subset, then the peak would be considered $CD4^+$ T-specific. For gene-based analyses, HOMER was used to assign each ATAC-seq peak to the nearest TSS, as measured from the peak center. To improve confidence on these annotations, gene-based analyses were further restricted to include only peaks located within 100 kb of their corresponding TSS. ATAC-seq peaks were also annotated using gene sets provided by curated immune function-related co-expression modules[13]. These gene sets comprise 28 modules defined from multiple compiled transcriptomic data sets, which were originally annotated based on expert knowledge of representative functions of the gene ensemble in each module. In this study, we have preserved and used these annotations to test for enrichment of these modules in gene sets of interest, such as the set of genes associated to chromatin peaks gaining or losing accessibility with aging. We assessed enrichment using the hypergeometric test followed by Benjamini-Hochberg FDR adjustment for P-values. Further functional enrichment analyses were carried out using Wikipathways pathways[51], immune modules[20], gene sets from DICE database[10] and single cell RNA-seq data in PBMCs. Gene sets from PBMC scRNA-seq data is driven from one-vs-all cell cluster comparisons. First, we identified 17 clusters from PBMC scRNA-seq data (n=26 samples) using the Louvain clustering in the ScanPy toolkit[52]. These clusters were manually inspected and assigned to different cell types by studying the expression of known marker genes. For each cluster, differentially expressed genes were identified using one-vs-all approach based on T-test followed by FDR. Marker genes for a cluster (or cell population) were found by using FDR <=5% and logFC > log2(1.25) using differential analyses results. Similarly, marker genes from the DICE database are obtained using their differential analyses results and the same cutoffs for cell-specific genes (FDR <=5% and logFC > log2(1.25)). Gene sets used in our differential analyses are provided as a supplementary table in **Table S14**. For each gene set, we tested for enrichment using the hypergeometric test, against a background defined by the set of genes that are expressed, as determined by RNA-seq data, or potentially expressed, as given by promoter accessibility, in PBMCs. We used the Benjamini-Hochberg FDR multiple test correction to assess significance of hypergeometric P-values.

Congruence between chromatin accessibility and transcription data: Gene expression (RNA-seq, see above) data was generated for a subset of subjects with ATAC-seq profiles (summarized in **Table S1**). These data were normalized to protein-coding transcripts, and annotated to ENSEMBL GRCh37 gene symbols. Genes for which at least three normalized reads per million were obtained in at least two samples were considered as expressed, all others removed prior to analysis. This resulted in a total estimate of 14,157 expressed genes in PBMCs. We built a data set comprising paired ATAC-seq and RNA-seq samples by matching promoter peaks to nearest gene (TSS) annotations, defining promoters as the regions within 1000 bp flanks of each TSS. Whenever multiple expressed genes were matched to the same promoter peak, the peak with the maximum fold change was chosen for visualization.

Inferring chronological aging trends: We used Autoregressive Integrated Moving Average (ARIMA) models as implemented in R on age-ordered normalized chromatin accessibility and expression data separately for each sex, to select genomic features (ATAC-seq peaks or mRNA-seq transcripts) to uncover significant chronological trends, as opposed to unstructured "noise" fluctuations undistinguishable from stationary data. Input data from all subjects in the study (see **Table S1**) were normalized as described for differential analyses, i.e., corrected for known batch effects using ComBat, and model-adjusted to correct for library size and unknown batch effects (i.e., surrogate variables) using EdgeR. Thus, ARIMA-modeled data contains variation due to age, sex, and error variance unaccounted for by batch and library size effects. For model fitting, genomic features were converted into z-ordered objects (using R package zoo) after averaging values obtained for the same sex and chronological age (in years), and into time series objects. Formatted time series were then analyzed using auto.arima (from the forecast R package), using stepwise search and Akaike Information Criterion (AIC) to select the best model. This algorithm scans a wide

range of possible ARIMA models and selects the one that satisfies the optimality criterion, i.e., the smallest AIC. Only non-seasonal models with a maximum difference (D) of 2 were considered in this study, such that a non-stationary trend the data can be modeled after integrating a stationary series once or twice. Overall, best-fitting ARIMA models based on chromatin accessibility or gene expression data included models with 0-7 AR, 0-5 MA, and 0-7 AR+MA parameters for accessibility and 0-4 AR, 0-3 MA, and 0-4 AR+MA parameters for expression. From these models, we chose for inspection only the ones carrying a "significant" trend, defined as those where (1) the difference order from stationary was higher than zero, and (2) at least one AR or MA coefficient was included in the model (i.e., $D>0 \cap AR+MA>0$). These criteria allow sampling a wide variety of trend patterns if they were present in the data. For accessibility data, 14,594 (18.7%) and 13,591 (17.4%) peak models had D=1 (none had D=2) in females and males respectively, out of which 13,297 (17%) and 13,295 (17%), respectively, also were estimated to have AR+MA>0, and hence chosen for further analyses. Out of the chosen peaks, 12,941 and 11,566 had only MA (9,082 in females, 8,696 in males) or AR (2,562 in females, 2,574 in males) coefficients, whereas only 4,196 (31.6%) and 4,181 (31.4%) were estimated to have two or more non-zero (AR+MA) coefficients in females and males, respectively. A total of 3,197 (4.1%) peaks were chosen in both sexes, whereas the remaining peaks were treated as sex-specific. For expression data, 1,367 (11.1%) and 1,665 (13.5%) models had D=1 (none had D=2) in females and males respectively, out of which 1,068 (8.6%) and 1,471 (11.9%), respectively, also were estimated to have AR+MA>0, and hence used in further analyses. Out of these, 1,359 and 832 had only MA (511 in females, 903 in males) or AR (480 in females, 372 in males) coefficients, whereas only 503 (36.8%) and 554 (33.3%) were estimated to have two or more non-zero (AR+MA) coefficients in females and males, respectively. A total of 180 (1.5%) peaks were chosen in both sexes, whereas the remaining peaks were treated as sex-specific.

Clustering and annotation of temporal peaks/genes: After selecting genomic features with a significant trend, we used their estimated parameters to fit the original data to reduce noise and facilitate the discovery of common trend patterns across multiple features. Fitted values were computed at the same chronological ages observed in the data for each sex, converted to z-scores for comparability, and then submitted to k-means clustering for aggregation into k sets of similar chronological aging patterns. Chosen features for each sex were clustered separately, and additionally features chosen as common to both sexes were concatenated as a single sequence of two age-ordered ages prior to normalization. This concatenation approach was designed to facilitate the detection of features with consistent chronological patterns across sexes. For clustering, we used the R-stats version of the k-means algorithm (kmeans), starting from nstart=1,000 random sets of k cluster centers and running each for max.iter=100 iterations. To choose k, we opted for a biologically informed criterion as opposed to a purely statistical one, after noting that criteria such as maximization of within- vs. between-cluster variance tended to select a large (>20) number of slightly different clusters, likely emphasizing small differences in ARIMA model parameters with little biological significance. Instead, we computed optimal clusters for values of k between 2 and 15 and calculated enrichment statistics for cell-specific features (i.e., cell-specific chromatin states for ATAC-seq, and cell-specific expressed genes for mRNA-seq data) for each cluster relative to all trending features, and asked whether adding clusters to the k=2 cluster case resulted in a gain of information demonstrated by cluster enrichment patterns qualitatively different from the patterns observed in absence of the extra clusters. In some cases, finding a cluster configuration satisfying this condition of biological discrimination required applying hierarchical clustering to collapse distinct k-means clusters. For chromatin accessibility, conservative application of these criteria led to the selection of k=5 and k=6 clusters for females and males, respectively, which were collapsed into 4 clusters in both cases (one closing, two opening with aging), and k=3 for peaks trending in both sexes (one closing and one opening in both sexes, plus one opening in females while closing in males). The same numbers of final clusters were defined based on gene expression.

TF motif enrichment analyses: To further explore functional associations of these clusters, we tested for enrichment of known and de novo transcription factor (TF) motifs in each chromatin accessibility cluster for female, male, and sex-pooled peak data, relative to all trending clusters for the same set of peaks. We used HOMER[49] to both detect de novo motifs and to test for enrichment of 1,388 motifs obtained from JASPAR CORE 2018 database[53] and from Jolma et al[54] SELEX-derived PWMs, corresponding to 680 distinct TFs. We used HOMER to assign a TF to each de novo motif found, based on sequence similarity to the 1,388 known motifs. From the pooled set of known and de novo motifs tested for each cluster, we used Benjamini-Hochberg method on enrichment P-values to estimate false discovery rates (FDR), and applied a 5% FDR significance threshold to select for the final set of enriched motifs. Since some motifs have similar consensus sequences and PWMs, prior to visualization of these results we grouped motifs into "families" defined as sets of motifs with nearly identical sequences, as determined by pairwise comparison of all 1,388 motif using MEME/TOMTOM[55], which tests whether two motif

sequences are more different than expected by chance. Using stringent 0.001% q-value and 5 E-value cutoffs, we identified 429 motif families with extremely similar consensus sequences, 319 of which were singletons (maximum family size=226 motifs).

Breakpoint analyses: We investigated systemic chronological signatures in temporal peaks by testing, in each cluster, for the existence of "breakpoints," i.e., short age intervals characterized by significant differences in accessibility in the intervals preceding and following the age interval. For each age t in the sampled age interval from tmin to tmax, we tested for mean difference in accessibility between subjects with ages in the intervals tmin-w vs. tmin+w, where w represents a variable window span parameter, and plotted the observed P-values (i.e., -log10 P, or loginvp) as a function of age (t) to identify maxima that suggested the presence of discrete breakpoints. These tests were carried out on normalized and model-adjusted accessibility data corresponding to the ATAC-seq peaks associated to each sex-specific and common cluster identified as trending by ARIMA as described above. Since there were many more peaks than subjects for any given comparison, we used PCA to reduce the dimensionality of each cluster to n=3 PCs, and used MANOVA on these three dimensions to compute P-values at each tested value of t. For any given value of w, offset values for tmin and tmax were adjusted to match available ages in the study. For example, a window span of 5 years would require a tmin=27 if the youngest available subject was 22 years old, and a tmax=83 if the oldest available subject was 90 years old. For a given value of w, results from tests contrasting younger vs. older intervals would vary depending on sample size volume and imbalance, with statistical power increasing with the size of the window span. To take advantage of this effect, we deployed a multi-scale algorithm where we carried out tests using w values ranging from 10 to 20 years in order to identify breakpoints that were maximally supported under multiple window spans. Due to sample sparsity and variation, however, tests carried out under varying w values may be unevenly affected by edge effects and influencing outlier points, which may result in strong significance of a comparison because of the presence of outliers and the partial overlap of a sampled interval with a breakpoint, limiting the ability of the method to precisely discover where such breakpoints may lie. To limit these effects and increase the robustness of the tests, we smoothed the loginvp distributions by fitting LOESS regressions to each comparison (i.e., each set of tests with the same w value) under a range of smoothing bandwidth parameters (i.e., bw = 0.25, 0.30, …, 0.70, 0.75). We combined the resulting eleven P-values at every sampled age using the Fisher's method, reapplied LOESS smoothing to the resulting distribution, and used numerical differentiation to determine whether each age was predicted to be minimum or a maximum. Finally, we marked every maximum as a "significant" breakpoint candidate if it satisfied both a parametric criterion, i.e. significance of the Fisher method-combined P-values (Chi-square test), and a heuristic criterion, namely whether the distance between this local maximum and the nearest minimum equaled or exceeded 25% of the value of the global maximum. The procedure described above results in a smoothed loginvp distribution for each w value, each comprising a series of points including maxima and minima, such that slightly different maxima can be estimated for different w values. Finally, we used Gaussian mixture modeling on the distribution of these maxima, as implemented in R-Mclust package, to group loginvp maxima obtained from different window spans into cohesive breakpoint intervals, whose medians and ranges we report herein for each cluster. Since breakpoints are independently calculated for each cluster, observed overlaps are likely the result of aging-related events with a genome-wide impact.

Analyses of public data from 500GG and MI projects: We obtained publicly available ELISA data measuring serum protein levels by the 500 Human Functional Genomics (500FG) consortium[11]. We only retained individuals who are matching our cohort in terms of the age span, which resulted in data from 267 individuals. These individuals are grouped together using the age brackets defined in our study: Young 22-40 years old, middle-aged: 41-64 years old, older: 65 years old. We compared data from 1) men and women at all age brackets; 2) young men to old men; and 3) young women to old women using Wilcoxon Rank Sum non-parametric test. Note that flow cytometry data from this same cohort was not publicly available; hence cannot be included into the analyses. Similarly, publicly available flow cytometry data from Milieu Intérieur Consortium[12] cohort was obtained. We used data that is already processed by this study and just used individuals whose ages are matching our cohort, which resulted in data from 892 individuals. We built linear models using R (lm function) to quantify the association between each flow cytometry measurement to age group (young, middle-aged, older), sex (F, M) and their interaction (age*sex). Significant associations with age (at FDR 5%) and with sex (at FDR 10%) are plotted in Figures S7D-E. No significant associations were detected with the interaction of sex and age at FDR 10%.

R Shiny Application: The R Shiny package[56] was used to create a webpage for the interactive visualization of the data from this study. Plots were generated using ggplot2[57], using graph aesthetics used throughout the manuscript

figures. Statistics for boxplots were calculated using the wilcox.test function in R and presented without correction for the multiple (n = 5) comparisons. Statistics for scatterplots were calculated by fitting a linear model with the lm function in R using the formula (measurement ~ age:sex + sex). For ATAC-seq data, only the peak closest to the gene TSS was considered.

REFERENCES

1 Castelo-Branco, C. & Soveral, I. The immune system and aging: a review. *Gynecol Endocrinol* **30**, 16-22, doi:10.3109/09513590.2013.852531 (2014).

2 Peters, M. J. *et al.* The transcriptional landscape of age in human peripheral blood. *Nature communications* **6**, 8570 (2015).

3 Jones, M. J., Goodman, S. J. & Kobor, M. S. DNA methylation and healthy human aging. *Aging cell* **14**, 924-932 (2015).

4 Moskowitz, D. M. *et al.* Epigenomics of human CD8 T cell differentiation and aging. *Science Immunology* **2**, eaag0192 (2017).

5 Ucar, D. *et al.* The chromatin accessibility signature of human immune aging stems from CD8(+) T cells. *J Exp Med* **214**, 3123-3144, doi:10.1084/jem.20170416 (2017).

6 Giefing-Kröll, C., Berger, P., Lepperdinger, G. & Grubeck-Loebenstein, B. How sex and age affect immune responses, susceptibility to infections, and response to vaccination. *Aging cell* **14**, 309-321 (2015).

7 Klein, S. L. & Flanagan, K. L. Sex differences in immune responses. *Nature Reviews Immunology* **16**, 626 (2016).

8 Abdullah, M. *et al.* Gender effect on in vitro lymphocyte subset levels of healthy individuals. *Cellular immunology* **272**, 214-219 (2012).

9 Fan, H. *et al.* Gender differences of B cell signature in healthy subjects underlie disparities in incidence and course of SLE related to estrogen. *Journal of immunology research* **2014** (2014).

10 Schmiedel, B. J. *et al.* Impact of Genetic Polymorphisms on Human Immune Cell Gene Expression. *Cell* **175**, 1701-1715. e1716 (2018).

11 Bakker, O. B. *et al.* Integration of multi-omics data and deep phenotyping enables prediction of cytokine responses. *Nature immunology* **19**, 776 (2018).

12 Piasecka, B. *et al.* Distinctive roles of age, sex, and genetics in shaping transcriptional variation of human immune responses to microbial challenges. *Proceedings of the National Academy of Sciences* **115**, E488-E497 (2018).

13 Chaussabel, D. *et al.* A modular analysis framework for blood genomics studies: application to systemic lupus erythematosus. *Immunity* **29**, 150-164 (2008).

14 Fulop, T. *et al.* Immunosenescence and inflamm-aging as two sides of the same coin: friends or foes? *Frontiers in immunology* **8**, 1960 (2018).

15 Olson, N. C. *et al.* Decreased naive and increased memory CD4(+) T cells are associated with subclinical atherosclerosis: the multi-ethnic study of atherosclerosis. *PLoS One* **8**, e71498, doi:10.1371/journal.pone.0071498 (2013).

16 Clave, E. *et al.* Human thymopoiesis is influenced by a common genetic variant within the TCRA-TCRD locus. *Science translational medicine* **10**, eaao2966 (2018).

17 Chen, Y., McCarthy, D., Robinson, M. & Smyth, G. K. (UsersGuide, 2014).

18 Kundaje, A. *et al.* Integrative analysis of 111 reference human epigenomes. *Nature* **518**, 317 (2015).
19 Feser, J. & Tyler, J. Chromatin structure as a mediator of aging. *FEBS letters* **585**, 2041-2048 (2011).
20 Chaussabel, D. & Baldwin, N. Democratizing systems immunology with modular transcriptional repertoire analyses. *Nature Reviews Immunology* **14**, 271 (2014).
21 Hidalgo, L., Einecke, G., Allanach, K. & Halloran, P. The transcriptome of human cytotoxic T cells: similarities and disparities among allostimulated CD4+ CTL, CD8+ CTL and NK cells. *American Journal of Transplantation* **8**, 627-636 (2008).
22 Wang, S. *et al.* S100A8/A9 in Inflammation. *Frontiers in Immunology* **9**, 1298 (2018).
23 Brockwell, P. J., Davis, R. A. & Calder, M. V. *Introduction to time series and forecasting*. Vol. 2 (Springer, 2002).
24 Johnson, J. L. *et al.* Lineage-determining transcription factor TCF-1 initiates the epigenetic identity of T cells. *Immunity* **48**, 243-257. e210 (2018).
25 Wöhner, M. *et al.* Molecular functions of the transcription factors E2A and E2-2 in controlling germinal center B cell and plasma cell development. *Journal of Experimental Medicine* **213**, 1201-1221 (2016).
26 Kijima, M. *et al.* Dendritic cell-mediated NK cell activation is controlled by Jagged2–Notch interaction. *Proceedings of the National Academy of Sciences* **105**, 7010-7015 (2008).
27 Hannum, G. *et al.* Genome-wide methylation profiles reveal quantitative views of human aging rates. *Molecular cell* **49**, 359-367 (2013).
28 Coleman, P., Finch, C. & Joseph, J. The need for multiple time points in aging studies. *Neurobiology of aging* **11**, 1-2 (1990).
29 Organization, W. H. *World health statistics 2016: monitoring health for the SDGs sustainable development goals*. (World Health Organization, 2016).
30 Hirokawa, K. *et al.* Slower immune system aging in women versus men in the Japanese population. *Immunity & Ageing* **10**, 19 (2013).
31 De Cecco, M. *et al.* L1 drives IFN in senescent cells and promotes age-associated inflammation. *Nature* **566**, 73 (2019).
32 Kaczorowski, K. J. *et al.* Continuous immunotypes describe human immune variation and predict diverse responses. *Proceedings of the National Academy of Sciences* **114**, E6097-E6106 (2017).
33 Rockwood, K. & Mitnitski, A. Frailty defined by deficit accumulation and geriatric medicine defined by frailty. *Clinics in geriatric medicine* **27**, 17-26 (2011).
34 Kuchel, G. A. Inclusion of Older Adults in Research: Ensuring Relevance, Feasibility, and Rigor. *Journal of the American Geriatrics Society* **67**, 203-204 (2019).
35 Robertson, D. & Williams, G. H. *Clinical and translational science: principles of human research*. (Academic Press, 2009).
36 Hardy, S. E., Kang, Y., Studenski, S. A. & Degenholtz, H. B. Ability to walk 1/4 mile predicts subsequent disability, mortality, and health care costs. *Journal of general internal medicine* **26**, 130-135, doi:10.1007/s11606-010-1543-2 (2011).
37 Podsiadlo, D. & Richardson, S. The timed "Up & Go": a test of basic functional mobility for frail elderly persons. *Journal of the American geriatrics Society* **39**, 142-148 (1991).

38 Rockwood, K., Awalt, E., Carver, D. & MacKnight, C. Feasibility and measurement properties of the functional reach and the timed up and go tests in the Canadian study of health and aging. *The journals of gerontology. Series A, Biological sciences and medical sciences* **55**, M70-73 (2000).

39 Buenrostro, J. D., Giresi, P. G., Zaba, L. C., Chang, H. Y. & Greenleaf, W. J. Transposition of native chromatin for fast and sensitive epigenomic profiling of open chromatin, DNA-binding proteins and nucleosome position. *Nature methods* **10**, 1213-1218, doi:10.1038/nmeth.2688 (2013).

40 Bolger, A. M., Lohse, M. & Usadel, B. Trimmomatic: a flexible trimmer for Illumina sequence data. *Bioinformatics*, btu170 (2014).

41 Li, H. & Durbin, R. Fast and accurate short read alignment with Burrows–Wheeler transform. *Bioinformatics* **25**, 1754-1760 (2009).

42 Zhang, Y. *et al.* Model-based analysis of ChIP-Seq (MACS). *Genome biology* **9**, R137 (2008).

43 Quinlan, A. R. & Hall, I. M. BEDTools: a flexible suite of utilities for comparing genomic features. *Bioinformatics* **26**, 841-842, doi:10.1093/bioinformatics/btq033 (2010).

44 Robinson, M. D. & Oshlack, A. A scaling normalization method for differential expression analysis of RNA-seq data. *Genome Biol* **11**, R25, doi:10.1186/gb-2010-11-3-r25 (2010).

45 Ewing, B., Hillier, L., Wendl, M. C. & Green, P. Base-calling of automated sequencer traces usingPhred. I. Accuracy assessment. *Genome research* **8**, 175-185 (1998).

46 Li, B. & Dewey, C. N. RSEM: accurate transcript quantification from RNA-Seq data with or without a reference genome. *BMC bioinformatics* **12**, 1 (2011).

47 Leek, J. T., Johnson, W. E., Parker, H. S., Jaffe, A. E. & Storey, J. D. The sva package for removing batch effects and other unwanted variation in high-throughput experiments. *Bioinformatics* **28**, 882-883, doi:10.1093/bioinformatics/bts034 (2012).

48 Qu, K. *et al.* Individuality and Variation of Personal Regulomes in Primary Human T Cells. *Cell Systems* **1**, 51-61 (2015).

49 Heinz, S. *et al.* Simple combinations of lineage-determining transcription factors prime cis-regulatory elements required for macrophage and B cell identities. *Molecular cell* **38**, 576-589 (2010).

50 Beekman, R. *et al.* The reference epigenome and regulatory chromatin landscape of chronic lymphocytic leukemia. *Nature medicine* **24**, 868 (2018).

51 Kelder, T. *et al.* WikiPathways: building research communities on biological pathways. *Nucleic Acids Res* **40**, D1301-D1307 (2012).

52 Wolf, F. A., Angerer, P. & Theis, F. J. SCANPY: large-scale single-cell gene expression data analysis. *Genome biology* **19**, 15 (2018).

53 Khan, A. *et al.* JASPAR 2018: update of the open-access database of transcription factor binding profiles and its web framework. *Nucleic acids research* **46**, D260-D266 (2017).

54 Jolma, A. *et al.* DNA-dependent formation of transcription factor pairs alters their binding specificity. *Nature* **527**, 384 (2015).

55 Bailey, T. L. *et al.* MEME SUITE: tools for motif discovery and searching. *Nucleic acids research* **37**, W202-W208 (2009).

56 Chang, W., Cheng, J., Allaire, J., Xie, Y. & McPherson, J. Shiny: web application framework for R. *R package version* **1** (2017).

57 Wickham, H. *ggplot2: elegant graphics for data analysis*. (Springer, 2016).

Figure 1

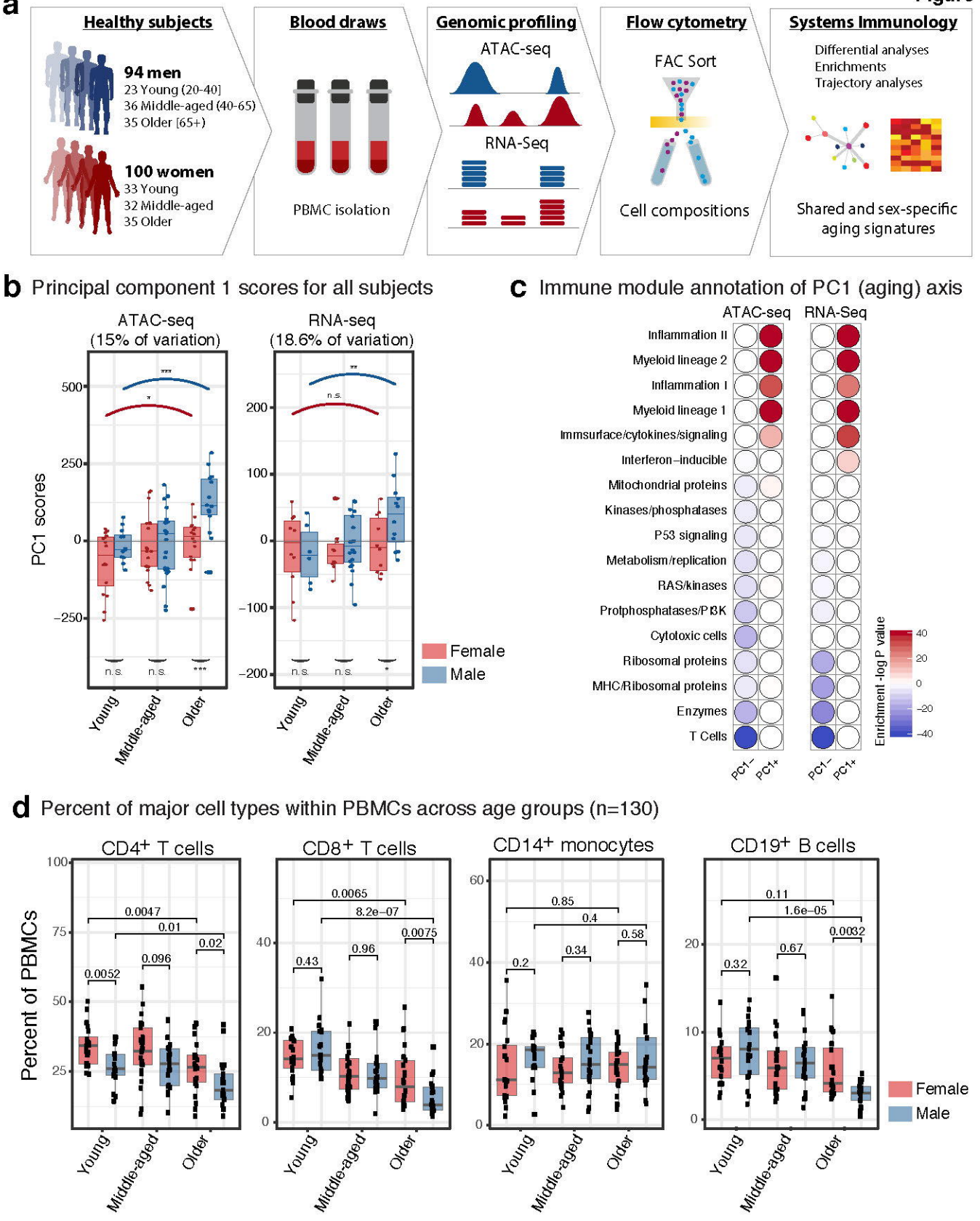
a
Healthy subjects
94 men
23 Young (20-40)
36 Middle-aged (40-65)
35 Older (65+)
100 women
33 Young
32 Middle-aged
35 Older
Blood draws
PBMC isolation
Genomic profiling
ATAC-seq
RNA-Seq
Flow cytometry
FAC Sort
Cell compositions
Systems Immunology
Differential analyses
Enrichments
Trajectory analyses
Shared and sex-specific aging signatures
b Principal component 1 scores for all subjects
ATAC-seq (15% of variation)
RNA-seq (18.6% of variation)
PC1 scores
Young
Middle-aged
Older
Female
Male
c Immune module annotation of PC1 (aging) axis
ATAC-seq
RNA-Seq
Inflammation II
Myeloid lineage 2
Inflammation I
Myeloid lineage 1
Immsurface/cytokines/signaling
Interferon–inducible
Mitochondrial proteins
Kinases/phosphatases
P53 signaling
Metabolism/replication
RAS/kinases
Protphosphatases/PI3K
Cytotoxic cells
Ribosomal proteins
MHC/Ribosomal proteins
Enzymes
T Cells
PC1−
PC1+
Enrichment -log P value
d Percent of major cell types within PBMCs across age groups (n=130)
CD4+ T cells
CD8+ T cells
CD14+ monocytes
CD19+ B cells
Percent of PBMCs
0.0052
0.0047
0.01
0.096
0.02
0.43
0.0065
8.2e−07
0.96
0.0075
0.2
0.85
0.4
0.34
0.58
0.32
0.11
1.6e−05
0.67
0.0032
Young
Middle-aged
Older
Female
Male

Figure 2

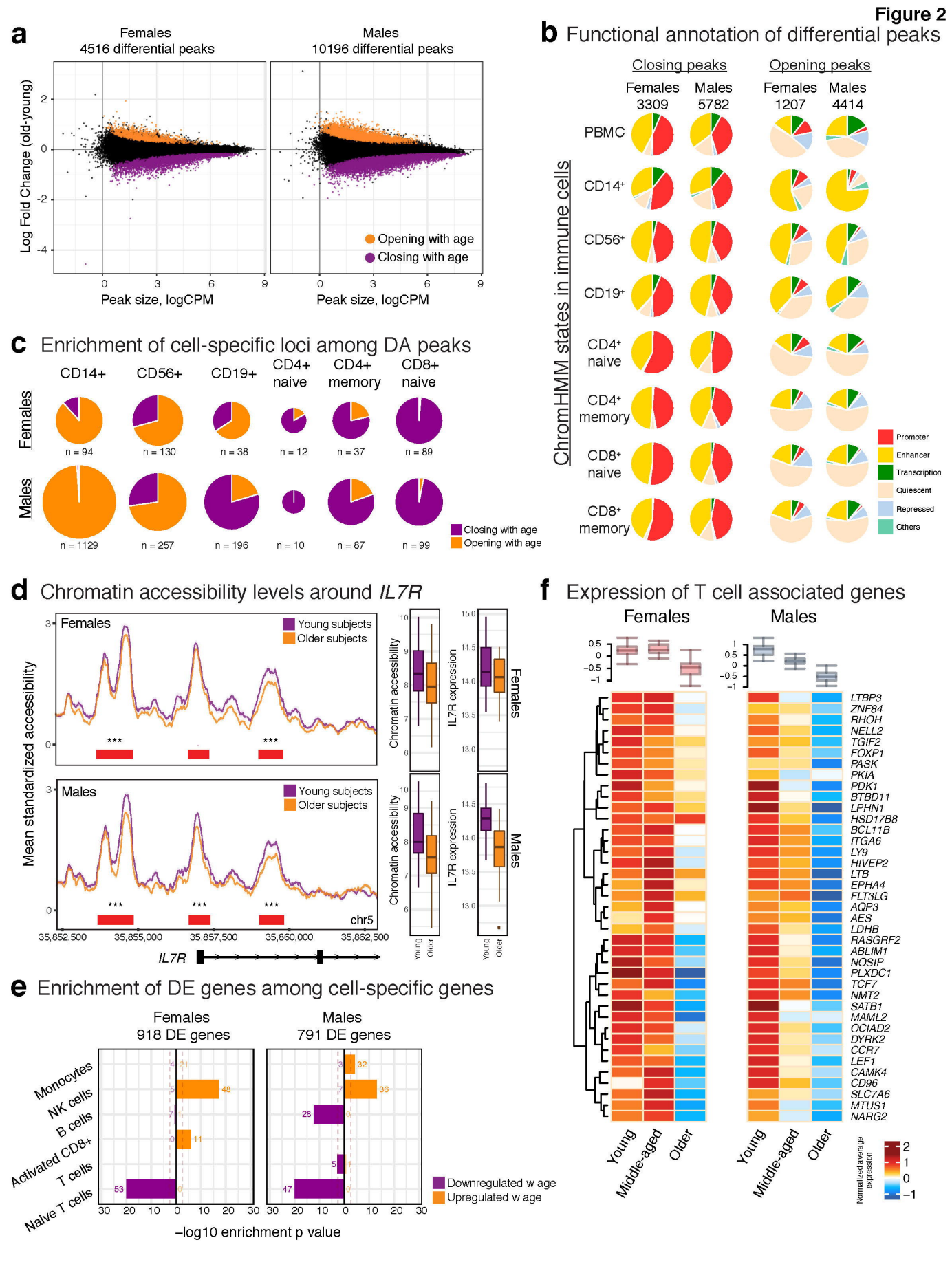
a
Females
4516 differential peaks
Males
10196 differential peaks
Log Fold Change (old-young)
Peak size, logCPM
Opening with age
Closing with age
b Functional annotation of differential peaks
Closing peaks
Opening peaks
Females 3309
Males 5782
Females 1207
Males 4414
ChromHMM states in immune cells
PBMC
CD14+
CD56+
CD19+
CD4+ naive
CD4+ memory
CD8+ naive
CD8+ memory
Promoter
Enhancer
Transcription
Quiescent
Repressed
Others
c Enrichment of cell-specific loci among DA peaks
CD14+
CD56+
CD19+
CD4+ naive
CD4+ memory
CD8+ naive
Females
Males
n = 94
n = 130
n = 38
n = 12
n = 37
n = 89
n = 1129
n = 257
n = 196
n = 10
n = 87
n = 99
Closing with age
Opening with age
d Chromatin accessibility levels around IL7R
Females
Males
Young subjects
Older subjects
Mean standardized accessibility
Chromatin accessibility
IL7R expression
Young
Older
chr5
35,852,500
35,855,000
35,857,500
35,860,000
35,862,500
IL7R
e Enrichment of DE genes among cell-specific genes
Females
918 DE genes
Males
791 DE genes
Monocytes
NK cells
B cells
Activated CD8+ T cells
Naive T cells
Downregulated w age
Upregulated w age
–log10 enrichment p value
f Expression of T cell associated genes
Females
Males
LTBP3
ZNF84
RHOH
NELL2
TGIF2
FOXP1
PASK
PKIA
PDK1
BTBD11
LPHN1
HSD17B8
BCL11B
ITGA6
LY9
HIVEP2
LTB
EPHA4
FLT3LG
AQP3
AES
LDHB
RASGRF2
ABLIM1
NOSIP
PLXDC1
TCF7
NMT2
SATB1
MAML2
OCIAD2
DYRK2
CCR7
LEF1
CAMK4
CD96
SLC7A6
MTUS1
NARG2
Young
Middle-aged
Older
Normalized average expression

Figure 3

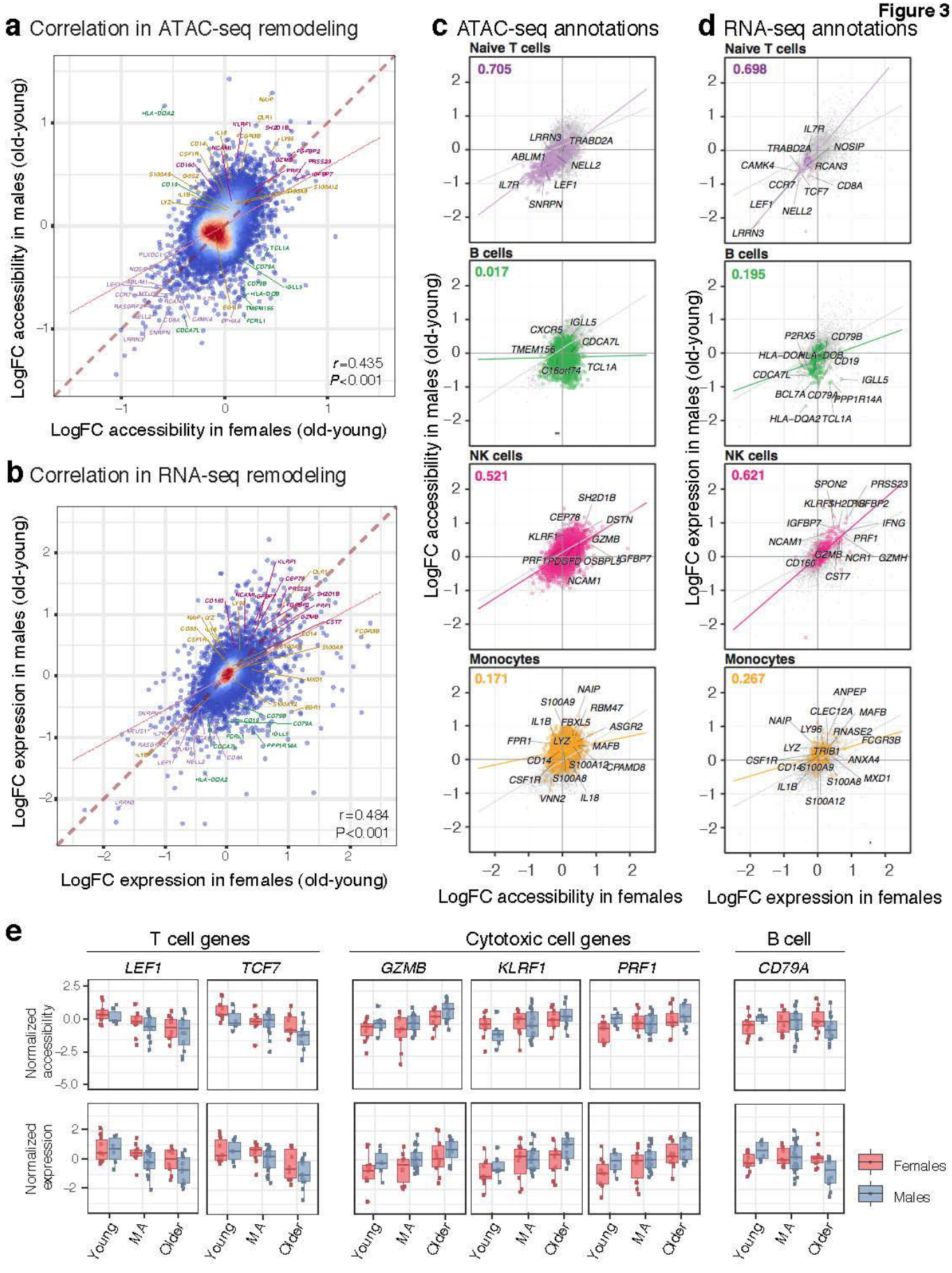
a Correlation in ATAC-seq remodeling
LogFC accessibility in males (old-young)
LogFC accessibility in females (old-young)
r=0.435
P<0.001
b Correlation in RNA-seq remodeling
LogFC expression in males (old-young)
LogFC expression in females (old-young)
r=0.484
P<0.001
c ATAC-seq annotations
Naive T cells
0.705
LRRN3
TRABD2A
ABLIM1
NELL2
IL7R
LEF1
SNRPN
B cells
0.017
IGLL5
CXCR5
CDCA7L
TMEM156
C16orf74
TCL1A
NK cells
0.521
SH2D1B
CEP78
DSTN
KLRF1
GZMB
PRF1
PDGFD
OSBPL5
IGFBP7
NCAM1
Monocytes
0.171
NAIP
S100A9
RBM47
IL1B
FBXL5
ASGR2
FPR1
LYZ
MAFB
CD14
S100A12
CPAMD8
CSF1R
S100A8
VNN2
IL18
LogFC accessibility in males (old-young)
LogFC accessibility in females
d RNA-seq annotations
Naive T cells
0.698
IL7R
TRABD2A
NOSIP
CAMK4
RCAN3
CCR7
CD8A
TCF7
LEF1
NELL2
LRRN3
B cells
0.195
P2RX5
CD79B
HLA-DOA
HLA-DOB
CD19
CDCA7L
IGLL5
BCL7A
CD79A
PPP1R14A
HLA-DQA2
TCL1A
NK cells
0.621
SPON2
PRSS23
KLRF1
SH2D1B
IGFBP2
IGFBP7
IFNG
NCAM1
PRF1
GZMB
NCR1
GZMH
CD166
CST7
Monocytes
0.267
ANPEP
CLEC12A
MAFB
NAIP
LY96
RNASE2
FCGR3B
LYZ
TRIB1
CSF1R
ANXA4
CD14
S100A9
S100A8
MXD1
IL1B
S100A12
LogFC expression in males (old-young)
LogFC expression in females
e
T cell genes
LEF1
TCF7
Cytotoxic cell genes
GZMB
KLRF1
PRF1
B cell
CD79A
Normalized accessibility
Normalized expression
Young
M.A
Older
Females
Males

Figure 4

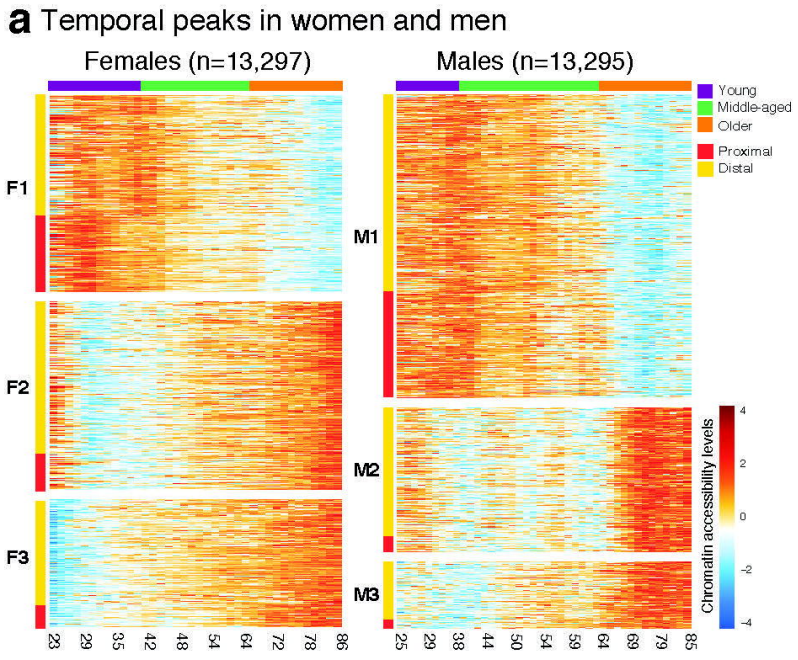
a Temporal peaks in women and men
Females (n=13,297)
Males (n=13,295)
Young
Middle-aged
Older
Proximal
Distal
F1
F2
F3
M1
M2
M3
Chromatin accessibility levels
23 29 35 42 48 54 64 72 78 86
25 29 38 44 50 54 59 64 69 79 85

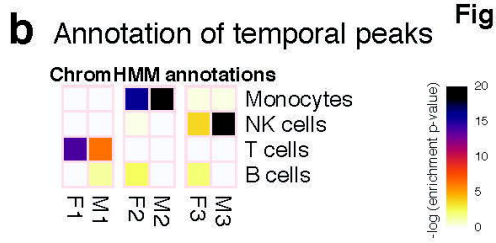
b Annotation of temporal peaks
ChromHMM annotations
Monocytes
NK cells
T cells
B cells
F1 M1 F2 M2 F3 M3
-log (enrichment p-value)
20 15 10 5 0

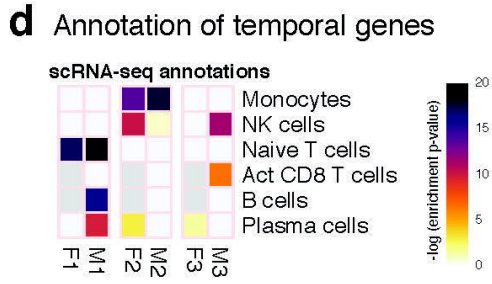
d Annotation of temporal genes
scRNA-seq annotations
Monocytes
NK cells
Naive T cells
Act CD8 T cells
B cells
Plasma cells
F1 M1 F2 M2 F3 M3
-log (enrichment p-value)
20 15 10 5 0

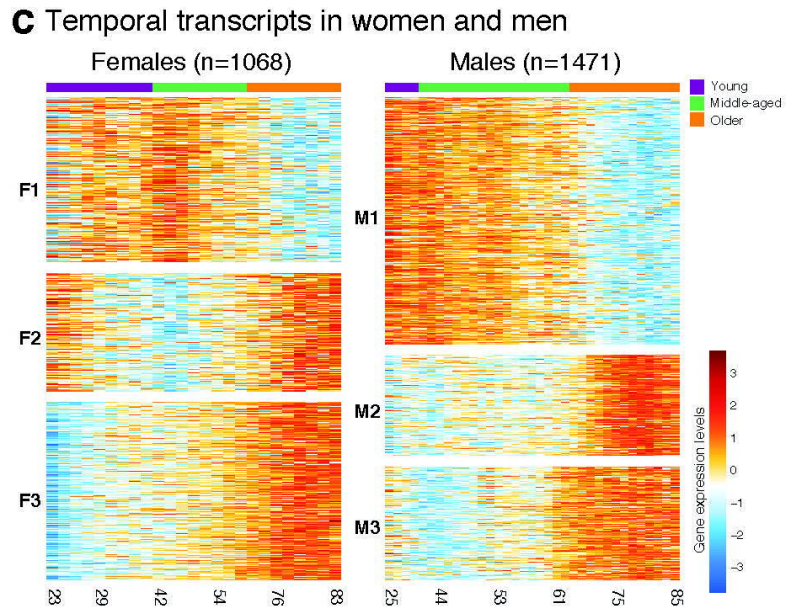
c Temporal transcripts in women and men
Females (n=1068)
Males (n=1471)
Young
Middle-aged
Older
F1
F2
F3
M1
M2
M3
Gene expression levels
23 29 42 54 76 83
25 44 53 61 75 85

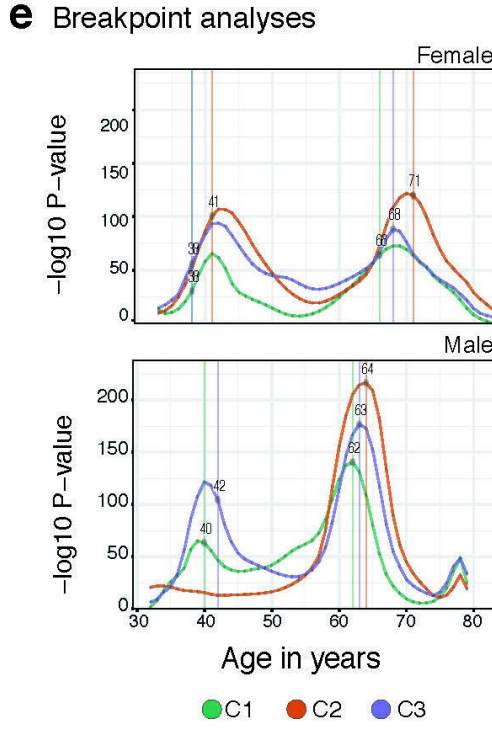
e Breakpoint analyses
Females
Males
−log10 P−value
Age in years
C1
C2
C3

Figure 5

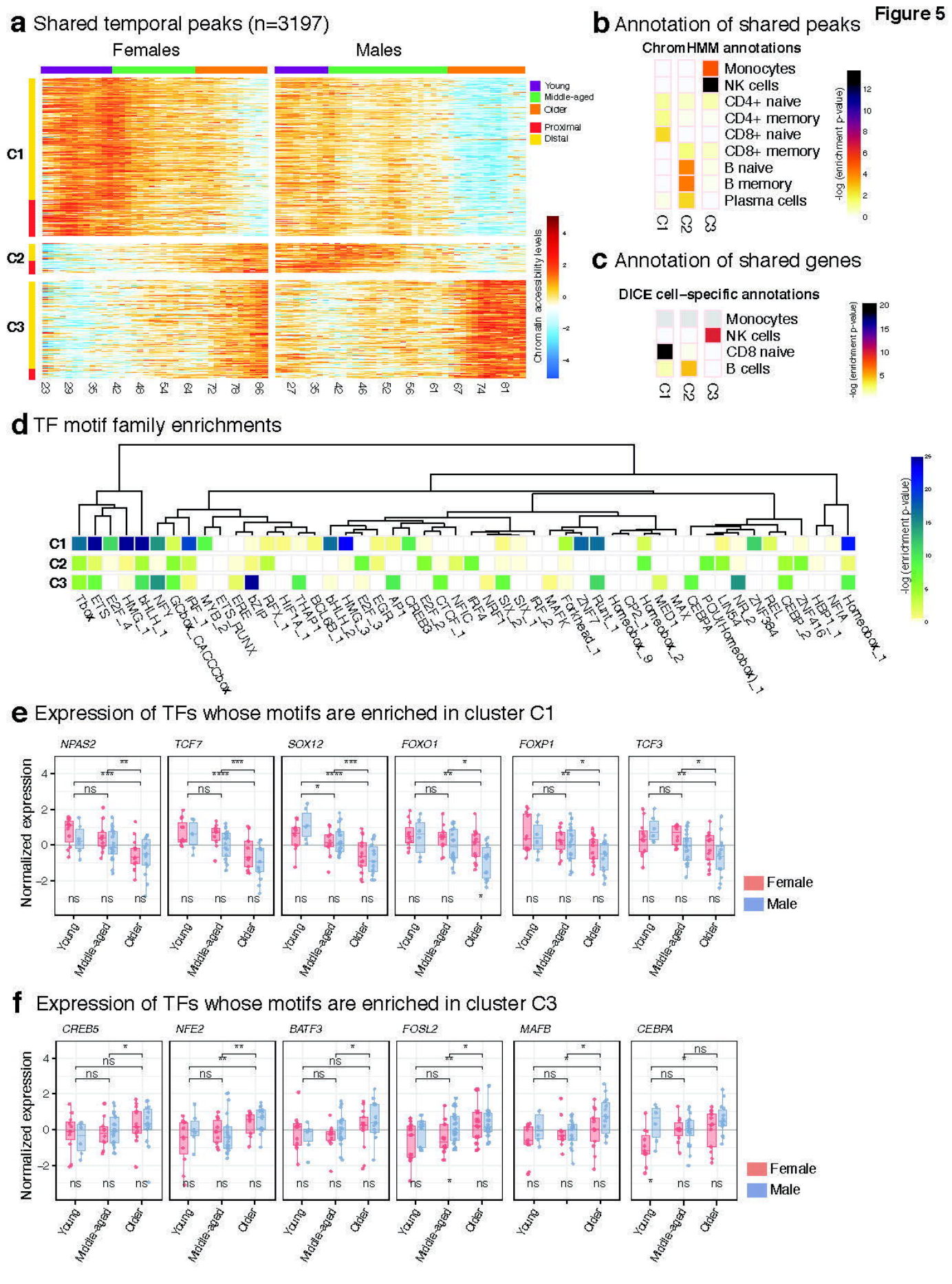
a Shared temporal peaks (n=3197)
Females
Males
Young
Middle-aged
Older
Proximal
Distal
C1
C2
C3
Chromatin accessibility levels
b Annotation of shared peaks
ChromHMM annotations
Monocytes
NK cells
CD4+ naive
CD4+ memory
CD8+ naive
CD8+ memory
B naive
B memory
Plasma cells
-log (enrichment p-value)
c Annotation of shared genes
DICE cell-specific annotations
Monocytes
NK cells
CD8 naive
B cells
d TF motif family enrichments
Tbox
ETS
E2F_4
HMG_1
bHLH_1
NFY
GCbox_CACCCbox
IRF_1
MTB_2
ETS_RUNX
ERE
bZIP
REX_1
HIF1A_1
THAP1
BCL6B_1
bHLH_2
HMG_3
E2F_3
EGR
AP1
CREB3
E2F_2
CTCF_1
NFIC
IRF4
NRF1
SIX_2
SIX_1
IRF_2
MAFK
Forkhead_1
ZNF7
Runt_1
Homeobox_9
CP2_1
Homeobox_2
MED1
MAX
CEBPA
POU(Homeobox)_1
LIN54
NR_2
ZNF384
REL
CREB_2
ZNF416
HBP_1
NF1A
Homeobox_1
e Expression of TFs whose motifs are enriched in cluster C1
NPAS2
TCF7
SOX12
FOXO1
FOXP1
TCF3
Normalized expression
Young
Middle-aged
Older
Female
Male
f Expression of TFs whose motifs are enriched in cluster C3
CREB5
NFE2
BATF3
FOSL2
MAFB
CEBPA
Normalized expression
Young
Middle-aged
Older
Female
Male

Figure 6

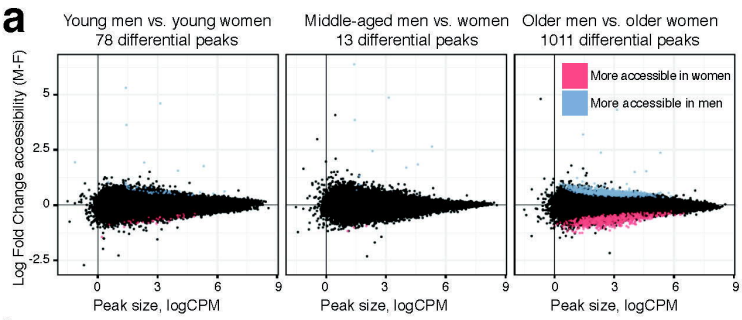

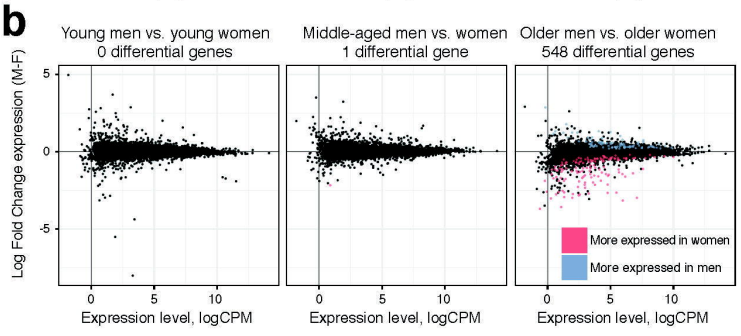

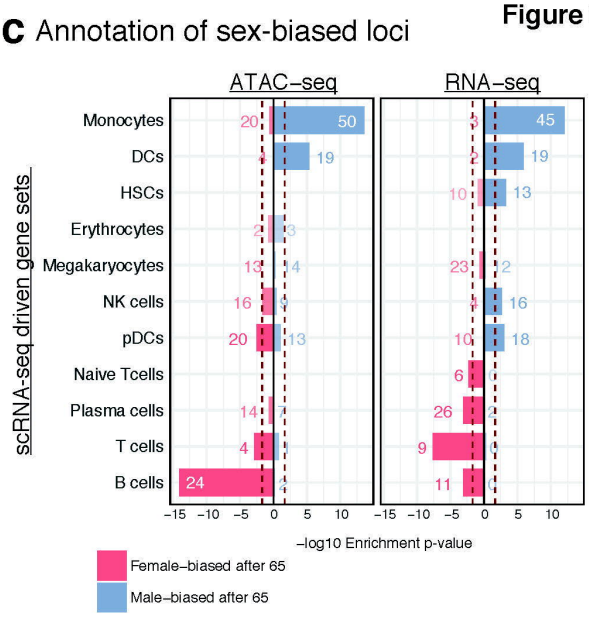

d
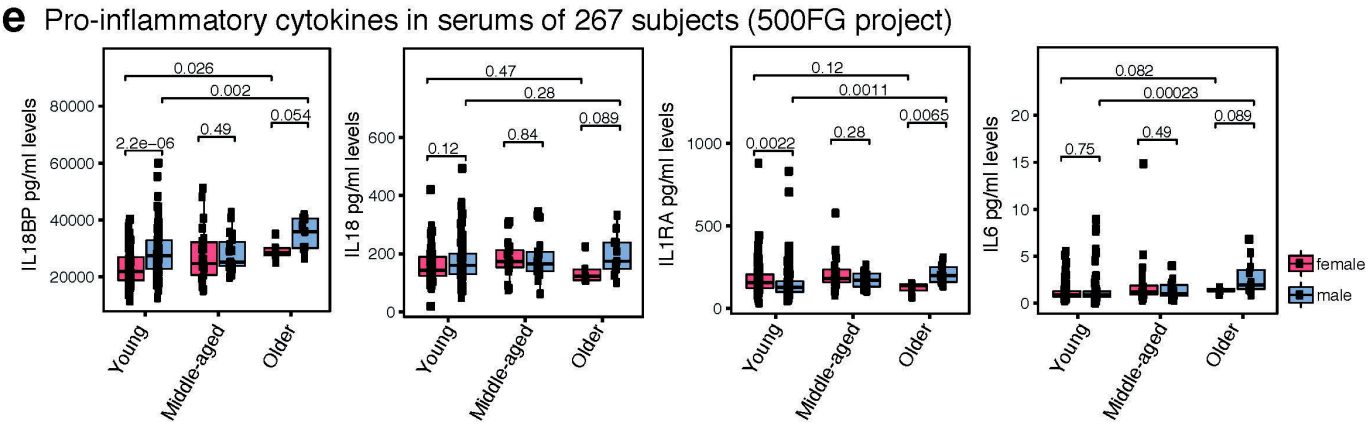
	RNA-seq/ATAC-seq* differences between old men and old women			Changes with age	
	Pathway/module name	FDR	No of hits/gene names	ATAC-seq	RNA-seq
Female-biased	IL-7 Signaling Pathway (WP205)	0.022	3/*JAK3, MYC, STAT5B*	▼,▼	NS,NS
Female-biased	PRC2 methylates,histones (WP3312)	6.67E-49	41/*HIST1H2AE, HIST1H2BD, HIST1H4I, HIST1H2AJ,...*	▼,▼	▲,NS
Female-biased	Interferon-inducible module*	0.00068	7/*IFIT3, IFI44, PARP14, EIF2AK2, TNFSF10, C1GALT1, ...*	NS,NS	NS,NS
Female-biased	B cells module*	1.61E-07	9/*PLEKHG1, TCF4, GGA2, SNX22, PAX5, CD22, BLNK, ...*	▲,▲	NS,NS
Male-biased	NOD pathway (WP1433)	0.027	3/*IL18, NAIP, RAC1*	NS,NS	NS,NS
Male-biased	Inflammation II module	2.93E-06	14/*H2AFY, CD302, MGST1, IL18, CPM, IRAK3, CD36, ...*	▲,▲	NS,NS
Male-biased	Inflammation I*	0.0048	10/*TREM1, FAM49A, SMURF1, IFRD1, THBS1, SLA, MAFB,...*	▲,▲	▲,▲
Male-biased	Inflammation II module*	0.00023	12/*CSF3R, CTSB, ASGR2, TFEB, RXRA, AOAH,LYN, CPM,...*	▲,▲	NS,NS